Technische Universität München

Fakultät für Medizin

Functionalized Hybrid Iron Oxide-Gold Nanoparticles Targeting Membrane Hsp70 Radiosensitize Triple-negative Breast Cancer Cells by ROS-mediated Apoptosis

Zhiyuan Wu

Vollständiger Abdruck der von der Fakultät für Medizin der Technischen Universität München zur Erlangung eines

Doktors der Medizin (Dr. med.)

genehmigten Dissertation.

Vorsitz: Prof. Dr. Susanne Kossatz

Prüfer*innen der Dissertation:

1. Prof. Dr. Gabriele Multhoff
2. Prof. Dr. Agnes Görlach

Die Dissertation wurde am 09. 03. 2023 bei der Technischen Universität München eingereicht und durch die Fakultät für Medizin am 15. 08. 2023 angenommen.

Table of Contents

1. Abstract

Triple-negative breast cancer (TNBC) refers to a specific type of tumor with a high level of aggressiveness and a poor prognosis. TNBCs are treated with multimodal therapies such as surgery, chemotherapy and irradiation (IR). The unfavorable clinical outcome of the disease can be attributed to both the normal tissue toxicity induced by IR and the presence of tumor cells that are resistant to radiation. To overcome radiation resistance, I analyzed the radiosensitizing potential of functionalized hybrid Gold (Au)-iron oxide (Fe_3O_4) nanoparticles (FeAuNPs). The presence of stress-inducible heat shock protein 70 (Hsp70) on the plasma membrane of highly aggressive tumor cells, including TNBCs, is widely acknowledged, whereas normal cells express Hsp70 only in the cytosol but not on the cell surface. Therefore, membrane-bound Hsp70 (mHsp70) acts as a tumor-specific target that might facilitate binding and internalization of FeAuNPs into tumor cells. In my thesis I functionalized FeAuNPs either with the Hsp70-specific, Tumor Penetrating Peptide TPP (TPP-PEG4-FeAuNPs) or a scrambled peptide as a control and compared the tumor targeting and uptake of these nanoparticles into mHsp70 positive tumor cells. I demonstrated a superior uptake of the TPP-functionalized FeAuNPs in both mHsp70 positive TNBC cell lines 4T1 (mouse) and MDA-MB-231 (human). I demonstrated that the TPP-functionalized FeAuNPs had a better uptake in both mHsp70-positive TNBC cell lines, 4T1 (mouse) and MDA-MB-231 (human). Moreover, a significant radiosensitizing effect could be achieved after incubation (24 h) with only the TPP-functionalized FeAuNPs, but not the FeAuNPs

functionalized with a non-specific scrambled peptide (NGL) or the non-conjugated FeAuNPs. The nanogold shell induces the releases of secondary electrons (Auger-electrons) as a result of IR and thereby breaks radioresistance. *In vivo*, the Fe3O4 core of the nanoparticles can act as a contrast agent, facilitating magnetic resonance imaging (MRI) of the tumor. When combined with irradiation, the TPP functionalized hybrid nanoparticles cause cell cycle arrest at the G2/M phase, enhance the production of reactive oxygen species (ROS), and consequently induce DNA double-strand breaks and apoptosis. Since the radiosensitizing effect was eliminated when co-incubated with the ROS inhibitor N-acetyl-L-cysteine (NAC), it is assumed that ROS mediated apoptosis is the reason for the increased apoptosis induced by TPP-PEG4-FeAuNPs.

2. Abbreviations

2D	Two-dimensional
3D	Three-dimensional
Ag	Silver
Au	Gold
APS	Ammonium Persulfate
BCA	Bicinchoninic acid
CD8a+	Cluster of differentiation 8a+
CeO_2	Cerium oxide
CFA	Colongenic formation assay
CT	Computed tomography
DAPI	4’,6-diamidino-2-phenylindole
DCFDA	2’,7’-dichlorofluorescin diacetate
ddH2O	Double-distilled water
DMSO	Dimethyl sulfoxide
DSBs	Double stranded breaks
EDTA	Ethylenediamine tetra acetic acid
ER	Estrogen receptor
FACS	Fluorescence-activated cell sorting
F-actin	Filamentous actin
FCS	Fetal calf serum
Fe_3O_4	Iron (II, III) oxide

FITC	Fluorescein isothiocyanate
Gd	Gadolinium
Gy	Gray
H2AX	H2A histone family member X
H2O2	Hydrogen peroxide
HO.	Hydroxyl radical
HCL	Hydrochloric acid
HER2	Human epidermal growth factor receptor 2
HIF1	Hypoxia-inducible factor 1
Hsp70	Heat shock protein 70
IL-5	Interleukin-5
IMRT	Intensity-modulated radiation therapy
IR	Ionizing radiation
JNK	C-Jun N-terminal kinase
LDL	Low-density lipoprotein
LEEs	Low-energy electrons
LET	Linear energy transfer
mHsp70	Membrane-bound Hsp70
MRI	Magnetic resonance imaging
NAC	N-acetyl-l-cysteine
NC	Nitrocellulose
NF-κB	Nuclear transcription factor-κB
NP	Nanoparticle

NR	Nanorod
NSCLC	Non-small cell lung cancer
OS	Overall survival
PBS	Phosphate buffered saline
PBL	Peripheral blood lymphocytes
Pd	Palladium
PEG	Polyethylene glycol
PFA	Paraformaldehyde
PI	Propidium iodide
PR	Progesterone receptor
RNase	Ribonuclease
RO.	Alkoxyl
ROO.	Peroxyl
ROS	Reactive oxygen species
RT	Room temperature
SD	Standard deviation
SDS-PAGE	Sodium dodecyl sulfate–polyacrylamide gel electrophoresis
TBST	Tris-buffered saline with Tween20
TEMED	Tetramethylethylenediamine
TNBC	Triple-negative breast cancer
TNF	Tumor necrosis factor
TPP	Tumor Penetrating Hsp70 Peptide
Zr	Zirconium

3. Introduction

3.1 Breast cancer

Breast cancer is the most frequent occurring malignant tumor in women globally. It accounts for approximately 24.5 % of all female malignant tumor and causes a mortality-to-incidence rate of 15.5 %. Breast cancer incidences were positive correlated with human development levels in different countries and area. In sub-Saharan Africa breast cancer incidences in females are estimated to be 30/100,000, whereas in Western Europe and North America, the incidence is 70/100,000 (Sung et al., 2021). In the United States and the European Union, the median age at diagnosis of breast cancer is around 40 years, which is 10 years later than in China (Song et al., 2014). An earlier onset of menarche and a later onset of menopause, a greater height, smoking and family history amplifies the probability of developing breast cancer (F. Chen et al., 2022; R. Qiu, Zhong, Hu, & Wu, 2022). On the other hand, breastfeeding decreased the risk of breast cancer (Bothou et al., 2022). The annual incidence of breast cancer in females aged 20-29 years increases by approximately 2 % each year, resulting in a higher proportion of breast cancer cases among young women (Miller et al., 2020), and patients with breast cancer at an age <25 usually have a worse prognosis (L. Li et al., 2021).

3.2 Triple-negative breast cancer (TNBC)

As a special subtype of breast cancer, TNBC refers to lack of estrogen receptor (ER),

progesterone receptor (PR), and human epidermal growth factor receptor 2 (HER2) expression. TNBC represents approximately 10 % to 20 % of all breast cancer subtypes (Bareche et al., 2020). For ER, two main subtypes, ER-α and ER-β exist (Mashat, Zielinska, Holly, & Perks, 2021). ER-α regulates oncogenes like cyclin D1 and c-Myc to promote breast cancer cells proliferation (Mawson et al., 2005). Low-density lipoprotein (LDL) is a risk factor of breast cancer and targeting of ER-β can reduce the impact of LDL in breast cancer patients (Mashat et al., 2021). PR is involved in the female menstrual cycle by binding to progesterone (Taraborrelli, 2015). Its synthesis is regulated by estrogen in both, normal and cancer cells (Silva et al., 1983). As a receptor tyrosine kinase, HER2 is expressed on the cell surface and is a member of the ErbB protein family. (Erickson, Zeybek, Santin, & Fader, 2020). Cancers with HER2 overexpression are often treated with a HER2-targeting therapy (Tsurutani et al., 2020).

Compared with other types of breast cancer at an equivalent T/N/M stage, patients with TNBC have significantly lower overall survival (OS) (X. Li et al., 2017). TNBC often migrates to brain and visceral organs due its high aggressivity, with metastatic patients having a median survival of only 13.3 months (Bardia et al., 2021; Lin et al., 2008). Due to the absence of targeting receptors, TNBC is unresponsive to therapies that rely on molecular or endocrine mechanisms(Yin, Duan, Bian, & Yu, 2020). Although ionizing radiation (IR) is a standard component of multimodal therapy for the vast majority of TNBC patients, the presence of radiation-resistant tumor cells and the risk of off-target toxicities often hinder the success of treatment outcomes (He et al., 2018).

Therefore, a high medical need exists for more targeted and effective radiation methods that minimize toxicity to normal tissues and increase the radiosensitivity of tumor cells.

3.3 Heat shock protein 70

The efficacy of targeted therapies in cancers depends on targets which is highly expressed in tumor cells and specifically presented on membrane. Heat shock proteins (HSPs) satisfy these criteria and can be effective and precise targets for therapy. (Bashiri Dezfouli et al., 2021; Dezfouli et al., 2022; Weidle, Maisel, Klostermann, Schiller, & Weiss, 2011). Following stress, cells significantly increase the synthesis of HSPs, whereas the synthesis of other proteins is generally downregulated. HSPs are classified into various families, such as Hsp40, Hsp60, Hsp70, Hsp90, and Hsp110, based on their estimated molecular weights (Vulczak, Catalao, Freitas, & Rocha, 2019). The 72 kDa Hsp70, also known as Hsp70-1, HspA1A, #3303, is highly conserved in evolution(Kimm et al., 2020) and frequently overexpressed in multiple cancer types, including breast cancer. Contrary to normal cells, many types of tumor cells, exhibit abundant expression of Hsp70 on their plasma membrane, making it a specific target for the tumor. Elevated levels of Hsp70 expression, both on the plasma membrane and in the cytoplasm, have been found to be positively associated with increased tumor aggressiveness(Multhoff et al., 1995; Stangl, Tontcheva, et al., 2018). Hsp70 can protect cancer cells from apoptosis (C. Zhang, Li, & Zhao, 2022), supports folding and unfolding of proteins and their transport across membranes. It was shown that Hsp70

protects tumor cells from apoptosis by an interference with members of the tumor necrosis factor (TNF) family (Giri et al., 2021). Hsp70 mediates promotion of angiogenesis which is crucial for tumor proliferation and migration (Kabakov & Gabai, 2021). Hsp70 is essential for the activation of Hypoxia-inducible factor 1 (HIF1). The knockdown of Hsp70 blocks HIF-1 induction upon hypoxia and finally suppresses the expression of vascular endothelial growth factor (VEGF) (Colvin et al., 2014). Interleukin-5 (IL-5) is another angiogenic activator. IL-5-induced angiogenic responses are associated with a dysfunction in HSP70-1 in knockout mice (Park et al., 2017).

Compared to HER-2, the turnover rate of membrane-bound Hsp70 (mHsp70) increases from hour range to minute range as it moves from the membrane into the cytosol. It is expected that nanoparticles designed to target mHsp70 will be rapidly internalized (Stangl, Gehrmann, Riegger, et al., 2011). Furthermore, following therapeutic interventions including radiochemotherapy, mHsp70 expression increases on various types of tumor cells but not on normal tissues (Gehrmann et al., 2014). Due to this stress-inducible, tumor-specific mHsp70 expression and its quick turnover rate (Stangl, Gehrmann, Riegger, et al., 2011) it appears that mHsp70 to be an optimal target for the internalization of NPs functionalized with an Hsp70-targeting agent like the monoclonal antibody cmHsp70.1 or Hsp70-targeting peptides.

3.4 Gold nanoparticles

The functional properties of gold nanoparticles depend on their size, surface chemistry and aggregation status (Enea et al., 2021; X. Li et al., 2021). AuNPs are quite inert,

show a low toxicity and a high stability, and can easily be conjugated to biomolecules. These properties qualify AuNPs as widely used tools in radiotherapy, immuno-therapy, drug delivery and imaging (Hassanen, Korany, & Bakeer, 2021; Oumano et al., 2021; Qin et al., 2021). Biogenetic gold nanoparticles (Au@MC38) combined with a local irradiation increases the proportion of cluster of differentiation 8a+ (CD8a+) dendritic cells and induces immunogenic cell death in MC38 tumor-bearing mice (Qin et al., 2021). AuNP–cisplatin conjugates improves the distribution of cisplatin in hepatic tumors and reduces the renal toxicity induced by cisplatin (Hassanen et al., 2021). Compared with traditional computed tomography (CT) contrast agent iodine, gold has a higher k-edge than iodine (80.7 keV to 33 keV), and therefore AuNPs provide an optimal image contrast at 120 kVp (Oumano et al., 2021).

Recently, the effectiveness of the cmHsp70.1 antibody in directing AuNPs to tumors was demonstrated through the enhanced accumulation and uniform distribution of NPs conjugated with cmHsp70.1 in mHsp70-positive tumor cells (Kimm et al., 2020). The radiosensitizing activities of AuNPs on tumor cells through secondary Auger electrons is well established (Huwaidi et al., 2021). The low energy of Auger electrons, which causes a high linear energy transfer (LET) over short distances (nm range), results in the formation of DNA double strand breaks (DSBs) and lethal damage in tumor cells(Ku, Facca, Cai, & Reilly, 2019). However, the average dose deposited by AuNPs is highly dependent on the distance from the DNA (Garnica-Garza, 2013). Additionally, the radiosensitizing effect of AuNPs is greatly influenced by their size. The effectiveness of AuNPs as a radiosensitizer depended on their size, smaller size providing a greater

increase in the mean dose linear energy, 2 nm nanoparticles can increase it up to 100 % while 100 nm nanoparticles can only increase it up to 40 % (Garnica-Garza, 2013).

3.5 Hybrid Gold Nanoparticles

The field of nanotechnology has made great progress with the creation of hybrid gold nanosystems, such as those made from combinations of gadolinium (Gd)-Au, silver (Ag)-Au, palladium (Pd)-Au, cerium oxide (CeO_2)-Au, and iron oxide (Fe_3O_4)-Au nanoparticles which have undergone both *in vitro* and in preclinical models (Akasaka, Nishi, & Niidome, 2021; Bhagat et al., 2018; R. Chen et al., 2021; Durand et al., 2021). "The field of nanotechnology has seen a new advancement with the creation of hybrid gold nanosystems, such as those made from combinations of gadolinium and gold, silver and gold, palladium and gold, cerium oxide and gold, and iron oxide and gold." These nanoparticles have been tested both *in vitro* and preclinical testing. Up to date Fe_3O_4-Au nanoparticles are among the most thoroughly researched hybrid nanoparticles with their physical characteristics and biocompatibility, these NP compositions are superior to other compositions(Cai, Miao, Li, & Fan, 2018). *In vivo,* the Fe3O4-AuNPs' Fe3O4 core is a contrast agent that enhances the magnetic resonance imaging (MRI) of tumors (Kang et al., 2019) and the gold shell has the capacity to improve the sensitivity of tumor cells to radiation therapy through the emission of secondary Auger electrons (Ngwa, Makrigiorgos, & Berbeco, 2012).

In 4T1 cells, Fe_3O_4-Au nanoparticles induced apoptosis through a p53 independent pathway. But in HCT116 and HUH7 cells apoptosis was induced through the p53/bcl-

2/casp-3 pathway (Katifelis et al., 2020). Fe_3O_4-Au nanoparticles were used as a signal indicator/multiplier and magnetic separator which can detect ochratoxin A with a high sensitivity and specificity (C. Wang et al., 2016). Gold nanorods (Au NRs) and Fe_3O_4 hybrid NPs increased the temperature by about 35 °C after 10 min exposure time with the NIR 808 nm laser They also show a high contrast enhancement in MRI and CT imaging (Feng et al., 2015).

3.6 Reactive oxygen species (ROS)

ROS include hydroxyl radical (HO.), superoxide ($O.2^-$), alkoxyl (RO.), peroxyl (ROO.) and hydrogen peroxide (H2O2) which were involved in the free radical chain reactions (Riley, 1994). The redox homeostasis in cancer cells is distinct from that of normal cells. High levels of ROS can be cytotoxic to cancer cells despite of they are pro-tumorigenic properties (Reczek et al., 2017). Hyperoside, one of the flavonoid glycosides, induces apoptosis in 4T1 cells via the ROS-mediated nuclear transcription factor-κB (NF-κB) Signaling Pathway (J. Qiu et al., 2019). ROS/c-Jun N-terminal kinase (JNK) pathway is another important pathway involved in ROS mediated apoptosis mechanisms in cancer cells (Z. Zhang, Zhang, et al., 2021).

AuNPs, similar to other high-Z nanoparticle materials, have the potential to significantly enhance the absorption of ionizing radiation by tumors, potentially increasing it up to 100-fold. The occurrence of this could result in alterations to both the quantity and type of highly reactive molecules, such as ROS (Huwaidi et al., 2021; Kuncic & Lacombe, 2018) which play a role in many critical signaling pathways (Jin, Wang, Deng, Liu, &

Liang, 2021; Weng et al., 2021), and the induction of DSBs (Yuan et al., 2020). Earlier research has shown that IR alone triggers the generation of ROS production, which causes oxidative stress and DNA damage(Y. Xu et al., 2021; Yalcin, Tekin, & Tigli Aydin, 2022). Furthermore, the combination of ionizing radiation and gold nanoparticles can enhance ROS production and DNA damage (Qin et al., 2021).

3.7 Hybrid Fe_3O_4-AuNPs functionalized with the Hsp70-peptide TPP

In this study, hybrid Fe3O4-Gold NPs functionalized with Hsp70-peptide TPP named TPP-PEG4-FeAuNP was developed. The aim of its development was to specifically eliminate the mHsp70 positive highly malignant TNBC cells. TPP is a 14-mer peptide which was originated from the C-terminal domain of Hsp70. It has the ability to bind to mHsp70-positive tumor cells with a comparable affinity to the full-length Hsp70 antibody cmHsp70.1, due to its similar binding characteristics to the oligomerization domain of Hsp70. Upon binding to mHsp70, the peptide is internalized and then accumulates within the cells (Stangl, Tei, et al., 2018). The targeting formulations are integrated with polyethylene glycol (PEG), a 4-mer chain to improve its stability by preventing self-aggregation of the TPP peptide (Hamidi, Rafiei, & Azadi, 2008). The TPP peptide-based PET tracer TPP-PEG24-DFO [^{89}Zr] was demonstrated to bind with high specificity to mHsp70-positive tumor cells [13]. In this study, TPP peptide functionalized hybrid TPP-PEG4-FeAuNPs binding and uptake capacity, as well as their potential to enhance radiation sensitivity in TNBC cell lines 4T1(murine) and MDA-MB-231(human) are tested.

4. Materials

4.1 Equipments

Name	Model	Supplier
Mechanical pipette, 1-channel, variable	Research plus	Eppendorf AG, Hamburg, DE
	0.1-10 µL	
	2-20 µL	
	20-200 µL	
	100-1000 µL	
Mechanical pipette, 8-channel, variable	Research plus	Eppendorf AG, Hamburg, DE
	10-100 µL	
	30-300 µL	
Stripettor Ultra	0.5-100 mL	Corning Inc., NY, US
CO_2 Incubator	Heracell 240i	Thermo Fisher Scientific, MA, US
Biological Safety Cabinets	ENVAIR eco safe Comfort Plus	ENVAIR Technology, Emmendingen, DE
Microcentrifuge	Fresco 21	Thermo Fisher Scientific, MA, US
General Purpose Centrifuge	Megafuge16	Thermo Fisher Scientific, MA, US
Irradiation machine	Gulmay RS225A	Gulamy Medical Ltd., Cambereley, UK

Absorbance Microplate Reader	ELx800	BioTek, Winooski, VT, US
Freezer	Herafreeze HFU 586 Basic, -86 °C, 510 Liter	Thermo Fisher Scientific, MA, US
Microscopy	ZEISS Primovert	Carl Zeiss AG, Oberkochen, DE
Microscopy	Leica, THUNDER Imager DMi8,	Leica Microsystems GmbH, Wetzlar, DE
Microplate reader	2030 Multilabel Reader	PerkinElmer Inc.Waltham, MA, US
Vortex mixer	Vortex-Genie 2	Scientific Industries, Inc., NY, US
Intelli-Mixer	RM-2L	ELMI, Riga, LV
Magnetic Stirrers	IKA RCT basic	IKA®-Werke GmbH & Co. KG, Staufen, DE
Scale	Ohaus precision balance Pioneer PX224	OHAUS Corporation, NJ, US
Electrophoresis Power Supply	EPS 301	Amersham Pharmicia Biotech, Amersham, UK
Trans-Blot Turbo Transfer System	Trans-Blot® Turbo™ Transfer System	Bio-Rad Laboratories, Inc., CA, US

ChemiDoc System	ChemiDoc MP	Bio-Rad Laboratories, Inc., CA, US
Flow cytometer	FACS Calibur/Calibur	BD Biosciences, NJ, US
Flow cytometer	MACSQuant Analyzer 9	Miltenyi Biotec, Bergisch Gladbach, North Rhine-Westphalia, DE

4.2 Consumables

Name	Model	Supplier
Cell culture bottles	TC bottle, T75	Sarstedt, Nümbrecht, DE
	TC bottle, T175	
Cell culture dishes	60 mm	TPP Techno Plastic Products AG, Trasadingen, CH
Cell Culture Test Plates	6-well	TPP Techno Plastic Products AG, Trasadingen, CH
	12-well	
	96-well	
Cell Scraper	Rotatable, 20 mm	TPP Techno Plastic Products AG, Trasadingen, CH
Slide A-Lyzer™ Dialysis Cassettes		Thermo Fisher Scientific, MA, US
Tube Racks	40 x cryo tubes with star foot	TPP Techno Plastic Products AG, Trasadingen, CH

	10 x 50 mL	
Cryo Tubes	Grad. max 1.5	TPP Techno Plastic Products AG, Trasadingen, CH
Cryo Boxes	81 x 2.0 mL	TPP Techno Plastic Products AG, Trasadingen, CH
Pipetman Diamond Tips	D10 Tips 10 µL	Gilson Inc., Middleton, WI, US
	D200 Tips 200 µL	
	D300 Tips 300 µL	
	D1000 Tips 1000 µL	
Cellstar Serological Pipette	5 mL	Greiner bio-one, Kremsmünster, AT
	10 mL	
	25 mL	
	50 mL	
Microreactiontube	1.5 mL	Eppendorf AG, Hamburg, DE
	2.0 mL	
Greiner centrifuge tubes	15 mL	Greiner bio-one, Kremsmünster, AT
	50 mL	
FACS Tube	Round Bottom Polypropylene Tube	Corning Inc., Corning, NY, US

Slide A-Lyzer™ Dialysis Cassettes	0.1-0.5 mL	Thermo Fisher Scientific, MA, US
Nitrocellulose membrane	0.45 µm, 30 cm x 3.5 m	Thermo Fisher Scientific, MA, US

4.3 Cells

MDA-MB-231 cells	HTB-26™, ATCC, VA, US
4T1 cells	CRL-2539^{TM}, ATCC, VA, US
PBL	Klinikum rechts der Isar, TUM

4.4 Hybrid Fe_3O_4-Au Nanoparticles

The hybrid nanoparticles are synthesized by Nanopartz Inc. Loveland CO, US. They are 4 nm in diameter. The hybrid nanoparticles are kept at a temperature of 4°C in a 5 mM citrate buffer for storage. Fe_3O_4 Au-CYS-NHS-PEG4-MAL-PEP (CNGLTLKNDFSRLEG) (Lot#K7312, NGL-PEG4-FeAuNPs, 2.7 mg/mL); Fe_3O_4 Au-CYS-NHS-PEG4-MAL (Lot#K7310, PEG4-FeAuNPs, 2.5 mg/mL); Fe_3O_4 Au-CYS-NHS-PEG4-MAL-PEP (CTKDNNLLGRFELSG) (Lot#K7311, TPP-PEG4-FeAuNPs, 2.3 mg/mL). The sublethal concentration of the different peptides conjugated and unconjugated NP formulations was determined by Alicia Hernandez-Schnelzer with colony formation assay. MDA-MB-231 cells are exposed to TPP-PEG4-FeAuNPs at concentrations ranging from 0 to 20 µg/mL (Figure 1 A). There were no significant differences in tumor cell viability observed between the conjugated and unconjugated

AuNPs up to a concentration of 2.5 µg/mL. MDA-MB-231 cells show a significantly lower survival rate when the concentration of both TPP-PEG4-FeAuNPs and NGL-PEG4-FeAuNPs reached 5.0 µg/mL. TPP-PEG4-FeAuNPs and NGL-PEG4-FeAuNPs up to 2.5 µg/mL also show no toxicity to 4T1 cells (Figure 1 B). For all NP formulations a concentration of 2.5 µg/mL are used for my experiments.

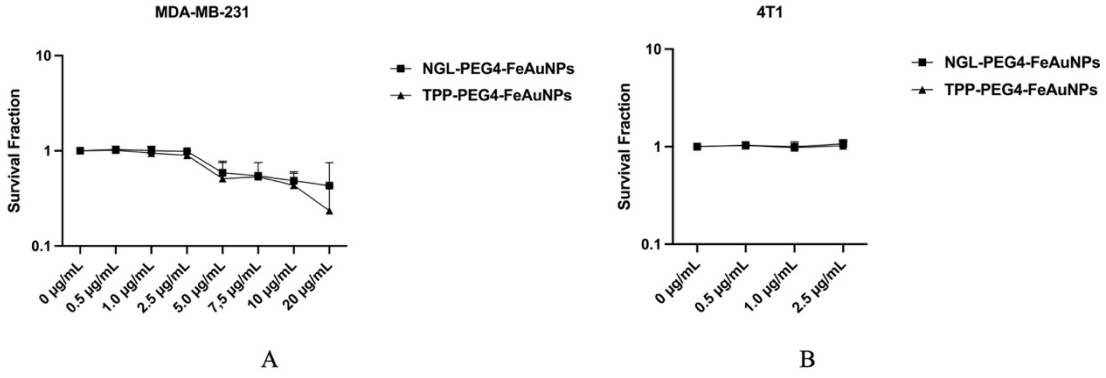

Figure 1. The survival fraction of MDA-MB-231(A) and 4T1(B) cells was assessed after exposure to NGL-PEG4-FeAuNPs and TPP-PEG4-FeAuNPs at varying concentrations. Data from Alicia Hernandez-Schnelzer. The results are presented as the mean values ± SD of 3 independent experiments.

4.5 Reagent

Reagent	Supplier
Phosphate Buffered Saline (PBS)	Sigma Aldrich, St. Louis, MO, US
Trypsin-EDTA solution	Sigma Aldrich, St. Louis, MO, US
RPMI 1640 medium	Sigma Aldrich, St. Louis, MO, US
Penicillin-streptomycin	GIBCO, Life Technologies, Carlsbad, US

FCS	GIBCO, Life Technologies, Carlsbad, US
L-glutamine	Sigma Aldrich, St. Louis, MO, US
Sodium pyruvate	Sigma Aldrich, St. Louis, MO, US
DMSO	Sigma-Aldrich, St. Louis, MO, US
Trypan Blue solution	Sigma Aldrich, St. Louis, MO, US
Ethanol	Supelco, Inc., PA, US
2-propanol	Otto Fischar GmbH & Co. KG, Saarbrücken, DE
Methanol	Supelco, Inc., PA, US
Ponceau S	Bio-Trend Chemikalien GmbH, Köln, DE
Propidium iodide	Merck KGaA, Darmstat, DE
Tris	Carl Roth, Karlsruhe, DE
Glycin	Carl Roth, Karlsruhe, DE
HCl	Sigma Aldrich, St. Louis, MO, US
Acrylamide/Bis-acrylamide, 30 % solution	Sigma Aldrich, St. Louis, MO, US
SDS	Carl Roth, Karlsruhe, DE
APS	Sigma Aldrich, St. Louis, MO, US
TEMED	Carl Roth, Karlsruhe, DE
Powdered Milk	Carl Roth, Karlsruhe, DE
Tween 20 Detergent	Merck KGaA, Darmstat, DE
Sodium azide	Sigma Aldrich, St. Louis, MO, US

RNase A	New England Biolabs, Frankfurt am Main, DE
Paraformaldehyde (PFA)	Thermo Fisher Scientific, MA, US
Rhodamine Phalloidin	Thermo Fisher Scientific, MA, US
Sodium carbonate buffer	Merck, KGaA, Darmstat, DE
Sodium azide	Sigma-Aldrich, St. Louis, MO, US
Fluorescein isothiocyanate isomer I	Sigma-Aldrich, St. Louis, MO, US
DAPI	Sigma-Aldrich, St. Louis, MO, US
D- (+)-Glucose	Sigma-Aldrich, St. Louis, MO, US
BD FACS Flow™ carrier fluid	BD Biosciences, NJ, US
N-Acetyl-L-cysteine	Abcam, Cambridge, UK
MG-132	Abcam, Cambridge, UK

4.6 Antibody

Anti-beta Actin antibody	Sigma-Aldrich, St. Louis, MO, US
Anti-gamma H2A.X (phospho S139) antibody	Abcam, Cambridge, UK
Anti-cmHsp70.1 antibody	multimmune GmbH, Munich, DE
FITC-labeled mouse IgG1	BD Biosciences, Heidelberg, DE

4.7 Kits

Kit	Catalogue No, Supplier

TACS Annexin V-FITC Apoptosis Detection Kit	4830-250-K, R&D Systems, Inc., MN, US
DCFDA/H2DCFDA-Cellular ROS Assay Kit	ab113851, Abcam, Cambridge, UK
Pierce BCA Protein Assay Kit	23227, Thermo Fisher Scientific, MA, US
Pierce ECL Western Blotting Substrate Kit	32106, Thermo Fisher Scientific, MA, US

4.8 Buffer

Buffer	Contents
Cell culture medium	500 mL RPMI 1640 medium
	50 mL FCS
	5 mL Penicillin/streptomycin
Cell frozen medium	90 % (v/v) cell culture medium
	10 % (v/v) DMSO
FACS buffer	90 % (v/v) PBS
	10 % (v/v) FCS
Western Blot Running Buffer	25 mM Tris
	192 mM glycine
	0.1 % SDS
Western Blot Transfer Buffer	25 mM Tris,
	192 mM glycine,

	10 % methanol
TBST	20 mM Tris
	137 mM NaCl
	pH 7.6 (with HCl)
	0.1 % (v/v) Tween 20
Western Blot Blocking buffer	TBST
	5 % (w/v) Milk
Annexin V FITC buffer (100 µL/sample)	ddH_2O 78 µL
	10X Binding Buffer 10 µL
	PI 10 µL
	Annexin V FITC 2 µL

4.9 Software

Software	Supplier
CellQuest Pro 6.0	BD Biosciences, Heidelberg, DE
Leica LAS X software 3.7.4	Leica Microsystems GmbH, Wetzlar, DE
GraphPad Prism 9	GraphPad Software, San Diego, CA, US
Image J 1.53a	National Institutes of Health, Maryland, US

5. Methods

5.1 Cell Culture

Two TNBC cell lines, 4T1 and MDA-MB-231, are used in present research. Both kinds of cells are cultured in complete medium prepared with RPMI 1640 medium, 10 % v/v heat-inactivated fetal calf serum (FCS) and 1 % v/v penicillin-streptomycin. Peripheral blood lymphocytes (PBL) are obtained from healthy donors' EDTA blood through density gradient centrifugation and cultured in RPMI-1640 medium supplemented with 1 mM sodium pyruvate and 2 mM L-glutamine. The Institutional Ethical Review Board of the Klinikum rechts der Isar granted approval for the blood taking procedure, and all volunteers provided written informed consent. All the cells are cultured at 37˚C with 5 % v/v CO2 and 95 % v/v relative humidity.

5.1.1 Thawing of cells

Before thawing cells, the water bath is preheated to 37°C first. Afterwards, frozen cells (stored in liquid nitrogen at -180°C) are taken out and quickly thawed in the preheated water bath. Subsequently, cell suspension is pipetted into a 15 mL falcon tube containing 4 mL cold complete medium and centrifuged at 500 rcf for 5 min at 4°C. Next, the supernatant is discarded and cells are resuspended with complete medium. Lastly, resuspended cell suspension is transferred into a fresh cell culture flask.

5.1.2 Passaging of cells

4T1 and MDA-MB-231 cells were passaged at a confluency of 80-90 %. All media and

buffer solutions are pre-warmed at room temperature for 30min. To detach cells, cells are washed with phosphate buffered saline (PBS) once before adding 0.15 % Trypsin-EDTA. Then cells are incubated with 0.15 % Trypsin-EDTA for 1-3 min at 37°C. Three volumes of FCS containing cell culture medium are added to cells to stop the effect of trypsin. Cells are transferred to a 15 mL Falcon tube and counted in a counting chamber. Before counting, cells were mixed with equal volume trypan blue, 10µL of the cell suspension mixer were transferred to counting chamber. Cells were counted with a 10x objective Zissis microscope. Trypan blue stained cells are considered as dead cells and are excluded. The final cell number per mL is determined by the average number of cells per large square and multiplied by $2 * 10^4$. For passaging, 0.5 x 10^6 cells are transferred into new cell culture flask (T25) for culture.

5.1.3 Freezing of cells

Cells are detached with 0.15 % Trypsin-EDTA as described above. The cell pellets are resuspended in FCS and Dimethyl sulfoxide (DMSO) (20 % in RPMI) medium (1:1) and transferred into CryoTube. CryoTube are kept in a pre-cold freezing container and stored at -80°C over night. After 24 to 48 hours, CryoTubes are moved to liquid nitrogen for preservation over an extended period.

5.2 Assessment of mHsp70 on TNBC Cells

FACS buffer is used to wash single cell suspensions. Afterward, cells are incubated under dark conditions and on ice, for a duration of 30 minutes with the FITC-conjugated cmHsp70.1 mAb. A FITC-labeled mouse IgG1 is used as an isotype-matched control.

After incubation, the cells are washed twice with flow cytometry buffer. The cells are resuspended again in 300 µL of flow cytometry buffer. Directly before measuring on a FACS Calibur instrument, 3 µL 0.02 mg/mL propidium-iodide (PI) was added to samples. Only viable cells and negative for PI staining were gated and analyzed. Data analysis was performed using CellQuest Pro 6.0 software.

5.3 Clonogenic Colony Formation Assay (CFA)

A 12-well cell culture plate is used to seed single cell suspensions containing 500 cells, which are then cultured overnight with 1 mL of cell culture medium. Then cells are incubated with 2.5 µg/mL hybrid nanoparticles for 24 hours, after which they are subjected to X-ray irradiation at 0, 2, 4, and 6 Gray (Gy) (Gulmay RS225A irradiation machine; 200 kV, 10 mA, dose rate 1 Gy/min). When colonies contain more than 50 cells, they are washed with PBS first. Next, pipet 1ml ice-cold methanol into each well to fix the cells for 10 min, and subsequently load 1ml 0.1 % crystal violet to stain the cells with for 10 min. Colony counting is performed for all colonies that has more than 50 cells. Each radiation dose's survival fraction was adjusted to that of the control group without nanoparticles, which is also exposed to a sham-irradiated dose of 0 Gy. The survival curves are fitted to the linear quadratic model performed with GraphPad Prism 9 software.

5.4 Nanoparticles labeled with FITC

The nanoparticles are diluted to 1 mg/mL with PBS before labelling. Add 1 M Sodium carbonate buffer to diluted Nanoparticles at a ratio of 1:10 v/v followed by 50 mL of

Fluorescein isothiocyanate (FITC) (10 mg/mL in 0.1 M Sodium carbonate buffer). The mixtures are incubated in the dark with gentle shaking at 4 °C for an overnight period. After incubation, conduct dialysis using Slide A-Lyzer™ Dialysis Cassettes. The nanoparticles concentration and dye/ nanoparticles ratio are calculated with microplate reader. Finally add 0.02 % w/v sodium azide to the mixer and keep them at 4°C.

5.5 Evaluation of Cellular Uptake of Nanoparticles Functionalized with TPP

The uptake of the nanoparticles mediated by mHsp70 was determined by using cancer cells (MDA-MB-231) that are positive for mHsp70 and normal cells (PBL) that are negative for mHsp70. Cells are seeded in a 6 well plate then cultured overnight with 2 mL of cell culture medium. On the next day, FITC-labeled NP formulations are added to the cells. After incubating with FITC-labeled NP formulations for 24 h, cells are measurements by flow cytometry. The uptake of hybrid nanoparticles was quantified by flow cytometry using a MACSQuant Analyzer 9.

5.6 Imaging the Cellular Uptake of Nanoparticles Functionalized with TPP

The visualize of nanoparticle internalization mediated by mHsp70 is determined by using cancer cells (MDA-MB-231) that are positive for mHsp70 and normal cells (PBL) that are negative for mHsp70. Cells are seeded and incubated overnight. The next day, the medium is changed with the one containing FITC-labeled TPP-PEG4-FeAuNPs (2.5 μg/mL). After 24 h incubation, the cells underwent twice washing with cold PBS, followed by fixation using paraformaldehyde (PFA) solution in PBS with a concentration of 4 % w/v at room temperature for 15 minutes. Following another

washing step, rhodamine-phalloidin (1 μg/mL) is used for filamentous actin (F-actin) and 4′,6-diamidino-2-phenylindole (DAPI) (2 μg/mL) is used for the nucleus of cells. They are incubated for 1 h at RT in the dark. Three-dimensional (3D) images are obtained with a fluorescence microscope (Leica, THUNDER Imager DMi8, Germany) with 63x objective. Leica LAS X software is used for image acquisition and processing.

5.7 Cell Cycle Analysis

The experiment involves seeding 4T1 and MDA-MB-231 cells in 6 well plates and allowing them to incubate overnight. After that, the cells are treated with After that, the cells are treated with different chemicals as shown in the paper for 24 h. Following that cells are irradiated with the Gulmay RS225A irradiation machine at 0 and 6 Gy. After 24 hours of irradiation, 500,000 cells were harvested through trypsinization. Afterwards, the cells are fixed in an ice-cold solution of 70 % methanol for an overnight period at 4°C. After being washed with FACS buffer, the cells are treated with the PI staining solution (50 μL RNAse A (0.2 mg/mL), 425 μL 0.1 % glucose/PBS) for a 30-minute incubation at 37°C. Prior to analysis, 25 μL PI (1 mg/mL) is added. The FACS Calibur instrument was used to determine the percentage of cell cycle distribution. Data analysis was performed using CellQuest Pro 6.0 software.

5.8 Analysis of Apoptosis with Flow Cytometry

The experiment involves seeding 4T1 and MDA-MB-231 cells in 6 well plates and allowing them to incubate overnight. After that, the cells are treated with different chemicals as shown in the paper for 24 h. Following that cells are irradiated with the

Gulmay RS225A irradiation machine at 0 and 6 Gy. After 24 hours of irradiation, 200,000 cells are harvested through trypsinization. After being washed with PBS, cells are mixed gently and incubated with Annexin V-FITC/PI buffer (100 µL/sample) in the dark for 15 min. Direct before analysis, 400 µL 1 * binding buffer are added. The FACS Calibur instrument is used to determine the percentage of apoptotic and necrotic cells. Data analysis is performed using CellQuest Pro 6.0 software.

5.9 Cellular Reactive Oxygen Species (ROS) Assay

The experiment involves seeding MDA-MB-231 cells in 6 well plates and allowing them to incubate overnight. After that, the cells are treated with different chemicals as shown in the paper for 24 h. Following the cells are irradiated with the Gulmay RS225A irradiation machine at 0 and 6 Gy. 24 h post irradiation, 200,000 cells are harvested through trypsinization. Cells are washed with PBS then incubated with 20 µM DCFDA for a 30-minute incubation at 37°C. Directly before analysis, 300 µL 1 * binding buffer are added. The FACS Calibur instrument is used to determine the ROS production. Data analysis is performed using CellQuest Pro 6.0 software.

5.10 Western Blot

After 1 hour of irradiation, cells are washed with ice-cold PBS for 1 time. From now on, all steps are performed on ice or at 4°C. Next, cells are treated with lysis buffer that included a protease inhibitor for 5 min. Cell scrapers are used to detach cells, after which the samples are transferred to 1.5 mL microtubes. The microtubes are kept on ice and vortexed for 3-times at 5-minute intervals. Afterward, the sample was

centrifuged at 13,000 rpm at 4°C for a duration of 15 minutes. Supernatant are kept as protein and the concentrations are determined with BCA kit. All the proteins are diluted with lysis buffer to 2.5 μg/μL. Next, 5 μL 5 * loading buffer is added to 20 μL supernatant. The mixer is heated at 95°C for 15 min and store at -20°C when finished.

Equal amount of protein solutions (50 μg/well) are pipetted into a 15 % SDS-PAGE gel and further resolved with a voltage of 80V. Successfully resolved proteins was transferred onto Nitrocellulose membrane (0.45 μm) via semi-dry transfer system with a voltage of 25 V and electric current of 1.0 A. The Nitrocellulose membrane are treated with a blocking solution with gentle shaking for 1 h at room temperature. All the antibodies are diluted with TBST containing 5 % nonfat milk. The primary antibodies are incubated with membrane overnight at 4°C with gentle shaking. The monoclonal anti-β-actin antibody is used as a loading control. The next day, the membranes undergo three times of washing with 1 * TBST, each lasting for 10 minutes. Protein bands are developed with ECL chemiluminescence substrate. Image J software is used for the band intensities analysis.

5.11 Statistical analysis

Data are presented as mean ± Standard deviation (SD) of n = experiments, with x indicating the number of independent experiments performed. GraphPad Prism 9 software was used for statistical analysis. The statistical significance was determined using t-tests with the normally distributed data. Results with $p<0.05$ were considered statistically significant.

6. Results

6.1 TNBC cells with high mHsp70-positive phenotype

In this study, FeAuNPs were functionalized either with the Hsp70-specific, Tumor Penetrating Peptide TPP (TPP-PEG4-FeAuNPs) or a scrambled peptide as an internal control. Before comparing the tumor targeting and uptake of these nanoparticle formulations, FITC-conjugated cmHsp70.1 antibody was used to determine the Hsp70 membrane status of TNBC cells by flow cytometry. The TNB cancer cells, 4T1 and MDA-MB-231 cells showed a mHsp70-positive phenotype on 63.1 ± 5.68 % (Figure 2 A) and 61.94 ± 7.88 % (Figure 2 B), respectively. Compared with TNBC cells, normal cells PBL showed a much lower mHsp70-positivity (3.25 ± 0.49 %; Figure 2 C). It is expected that Hsp70 peptide TPP-conjugated NPs target mHsp70 tumor cells with a similar high affinity like cmHsp70.1 antibody and that the fast turn-over rate of mHsp70 (Stangl, Gehrmann, Riegger, et al., 2011) will promote the specific uptake of FeAuNPs into TNBC cells.

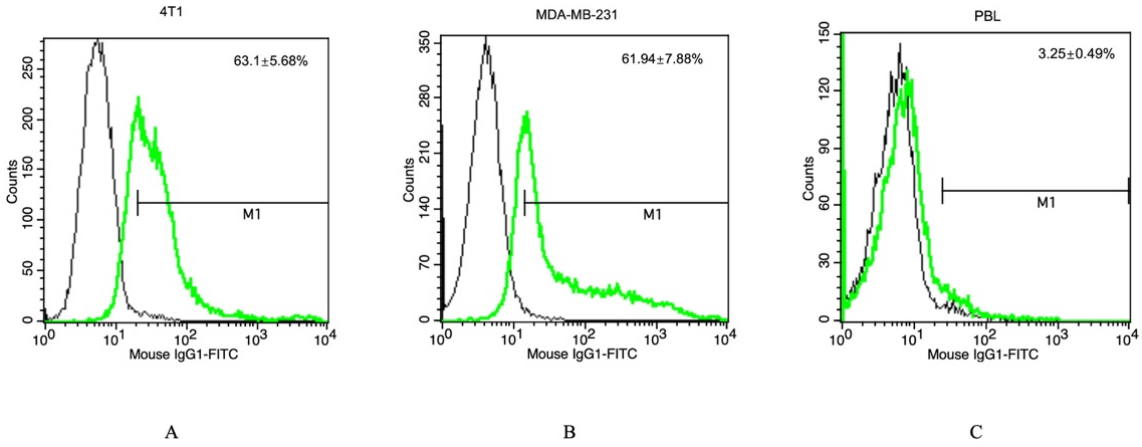

Figure 2. The mHsp70 statues of TNBC cells and PBL. FITC-labeled cmHsp70.1

antibody (represented by a green line) and an FITC-labeled mouse IgG1 control antibody (represented by a black line) are used to conduct flow cytometric analysis of 4T1 (A), MDA-MB-231 (B), and PBL (C), and the representative histograms are shown. The mean values ± SD from three independent experiments is presented in the upper right corner of each graph.

6.2 TPP Peptide Increases TNBCs Affinity to FeAuNPs

Based on Figure 1, it can be inferred that 2.5 μg/mL hybrid nanoparticles show no toxicity in TNBC cells. I also tested the toxic effects induced by the different FeAuNPs formulations in normal cells (PBL) by CCK-8 assay. NGL-PEG4-FeAuNPs and TPP-PEG4-FeAuNPs at a concentration of 2.5 μg/mL doesn't induce cell death in PBL (Figure 3).

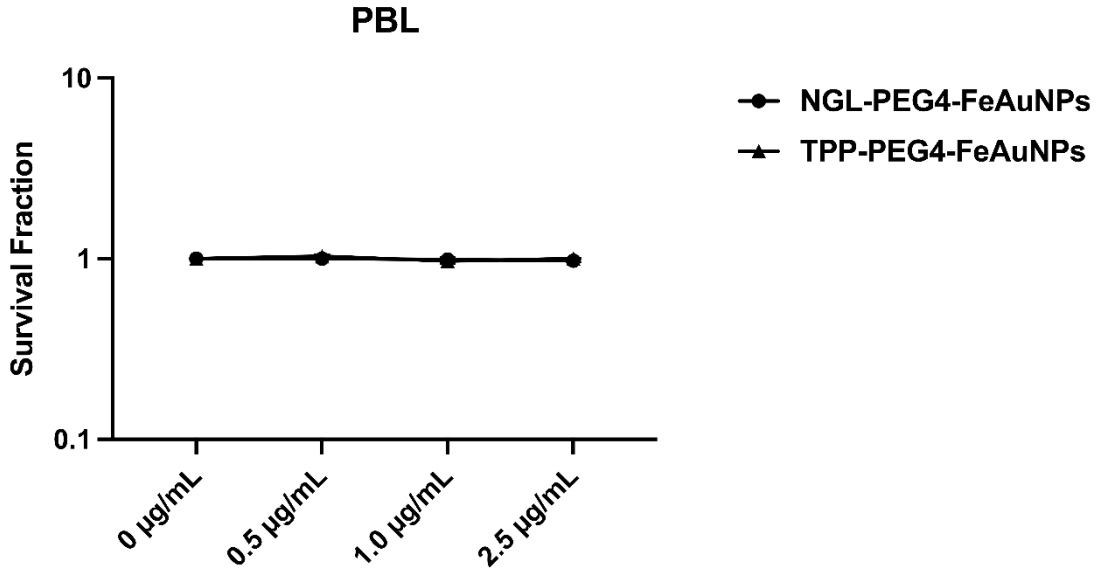

Figure 3. Hybrid nanoparticles show no toxic effects to PBL. NGL-PEG4-FeAuNPs

and TPP-PEG4-FeAuNPs are administered in concentration from 0 to 2.5 µg/mL for the treatment of PBL. The survival fraction of PBL is determined by CCK-8 assay. Results represent the mean values ± SD of 3 independent experiments.

It is expected that Hsp70 peptide TPP-conjugated NPs target mHsp70 on tumor cells with a high affinity like cmHsp70.1 antibody and the rapid turn-over rate of mHsp70 (Stangl, Gehrmann, Riegger, et al., 2011) will promote the specific uptake efficiency of hybrid nanoparticles by TNBC cells. To prove this hypothesis, the uptake capacity of the different nanoparticle formulations (NGL-PEG4-FeAuNPs, PEG4-FeAuNPs, TPP-PEG4-FeAuNPs) was analyzed comparatively in MDA-MB-231 cells by microscopy. As illustrated in Figure 4, after 24 h incubation, compared to other formulations, TPP-PEG4-FeAuNPs demonstrated the highest internalization and most homogeneous distribution in MDA-MB-231 cells, particularly around the nucleus.

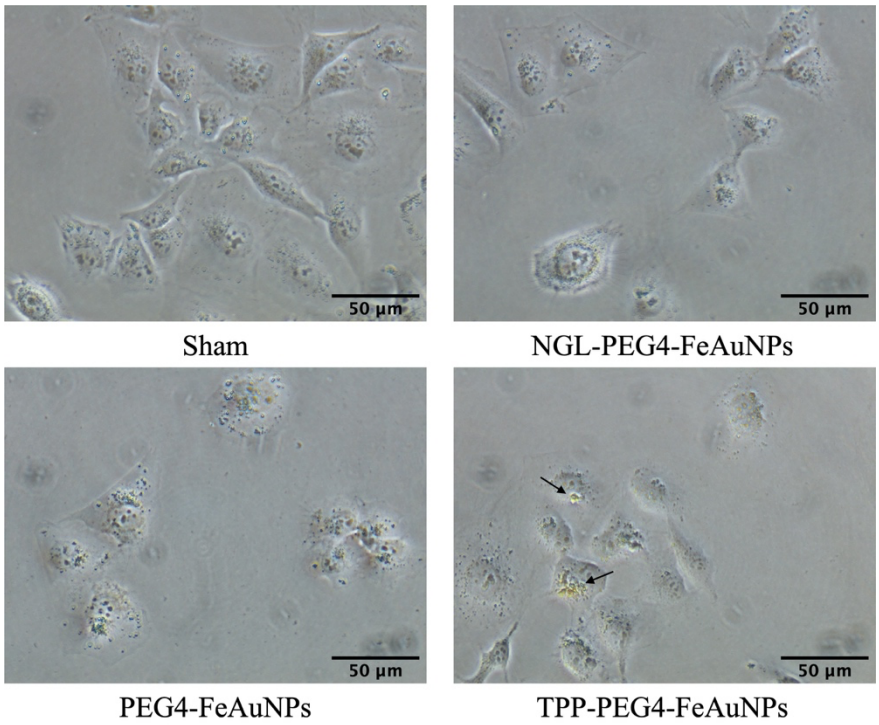

Figure 4. Representative images of MDA-MB-231 cells undergo sham or different nanoparticle formulations (NGL-PEG4-FeAuNPs, PEG4-FeAuNPs and TPP-PEG4-FeAuNPs, 2.5 µg/mL for 24 h) treatment. The presence of NPs accumulation within the MDA-MB-231 cells is indicated by black arrows.

As shown in Figure 2, 63.1 ± 5.68 % of MDA-MB-231 cells were found to be mHsp70-positive, while only 3.25 ± 0.49 % of PBL cells were mHsp70-positive, therefore they were considered as mHsp70-negative. FITC-labeled FeAuNPs were administered to both MDA-MB-231 cells and PBL to demonstrate that the internalization of TPP-PEG4-FeAuNPs into MDA-MB-231 tumor cells was mediated by mHsp70. After 24 h incubation, uptake of TPP-PEG4-FeAuNPs into the different cells was acquired by fluorescence microscopy (Figure 5 A, B). MDA-MB-231cells but not PBL showed a

significant uptake of TPP-PEG4-FeAuNPs. To quantify uptake of the different NP-formulations in cancer cells (MDA-MB-231) and normal cells (PBL), flow cytometry was used to determine FITC signal in the cells incubated with FITC- labeled FeAuNPs. As shown in Figure 5 C, TPP-PEG4-FeAuNPs were internalized only in mHsp70 positive MDA-MB-231 tumor cells, while NGL-PEG4-FeAuNPs were not taken up to a significant degree. In mHsp70 negative PBL, neither mHsp70-specific NPs (TPP-PEG4-FeAuNPs) nor non-specific control NPs (NGL-PEG4-FeAuNPs) were taken up.

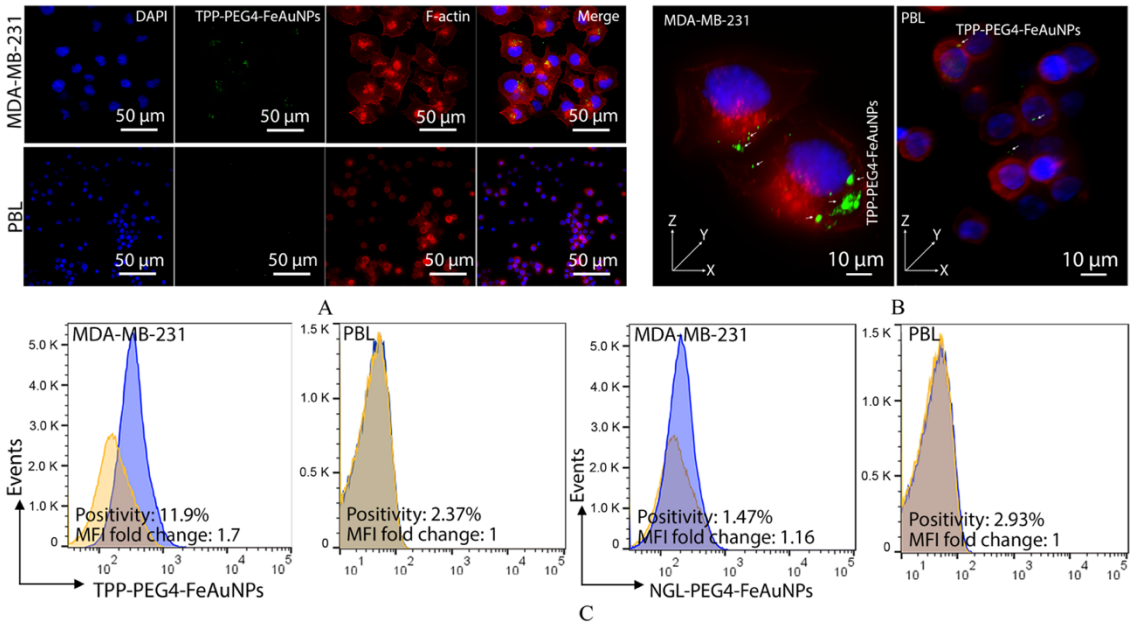

Figure 5. Uptake of TPP-PEG4-FeAuNPs by TNBC cells. (A, B) Fluorescence images demonstrate that mHsp70-positive MDA-MB-231 cancer cells specific uptake TPP-PEG4-FeAuNPs, whereas mHsp70-negative normal cells (PBL) do not show this effect. (B) Using fluorescence microscopy to acquire 3D images showing the uptake status of TPP-PEG4-FeAuNPs in MDA-MB-231 cells and PBL. (C) The results of flow cytometry assay quantified the uptake of TPP-PEG4-FeAuNPs and NGL-PEG4-FeAuNPs into

MDA-MB-231 cells and PBL. Experiments were repeated twice and representative data are presented.

6.3 TPP-PEG4-FeAuNPs Inhibit TNBCs proliferation by Radiosensitization effect

As shown in Figure 4 and Figure 5, mHsp70-specific NPs (TPP-PEG4-FeAuNPs) were significantly taken up by MDA-MB-231 cells. To prove the radiosensitization effect of TPP-PEG4-FeAuNPs after uptake colony formation assays were performed. All NP formulations were used at a concertation of 2.5 μg/mL. After incubating 4T1 (Figure 6A) and MDA-MB-231 (Figure 6B) cells with different NPs (TPP-PEG4-FeAuNPs, NGL-PEG4-FeAuNPs, and PEG4-FeAuNPs) for 24 hours, they were irradiated with doses of 0, 2, 4, and 6 Gy. When exposed to different radiation doses, only cells treated with TPP-PEG4-FeAuNPs exhibited lower survival. In another two NP formulations, no change in cell survival was found at all doses compared to cells of the sham group. These results suggest that TPP peptide targets mHsp70 on TNBC cells and thereby facilitates the internalization and accumulation TPP-PEG4-FeAuNPs into 4T1 and MDA-MB-231 tumor cells. When TPP-PEG4-FeAuNPs were taken up by TNBC cells, their proximity to the nucleus makes tumor cells more sensitive to ionizing radiation.

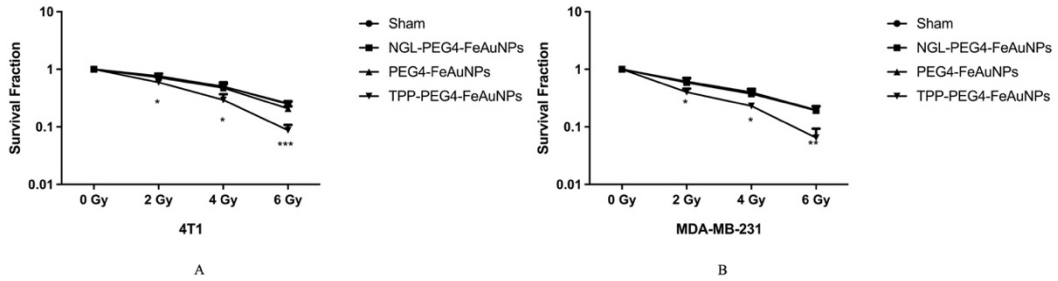

Figure 6. The survival fractions of TNBC cells 4T1(A) and MDA-MB-231 (B) are

determined by colony formation assays. Cells are treated with NGL-PEG4-FeAuNPs, PEG4-FeAuNPs, and TPP-PEG4-FeAuNPs (2.5 μg/mL for 24 h) or a sham treatment and followed by exposure to different dose of irradiation (0, 2, 4, 6 Gy). Significant differences are detected between the cells undergo sham treatment and TPP-PEG4-FeAuNPs treatment. Significance: *$p \leq 0.05$, **$p \leq 0.01$, ***$p \leq 0.01$; results represent the mean values ± SD of 3 independent experiments.

6.4 TPP-PEG4-FeAuNPs Induce Cell Cycle Arrest at G2/M in TNBCs

Radiation is well known to cause cell cycle arrest at the G2/M checkpoint (D. Xu et al., 2020). The radiosensitizing effect of hybrid Au-NPs on the cell cycle distribution was studied by flow cytometry. All NPs were used at a concertation of 2.5 μg/mL because this was defined as a non-lethal concentration. The NPs were added to 4T1 (Figure 7 A, B) and MDA-MB-231 (Figure 7 C, D) cells and left to incubate for 24 h before being exposed to a radiation dose of 6 Gy. As shown in Figure 7 A, B, 4T1 cells showed 13.65 ± 2.83 % G2/M phase ratio before any treatment. After irradiation with 6 Gy, the G2/M ratio increased to 23.95 ± 2.43 %. After being incubated with TPP-PEG4-FeAuNPs for 24 h followed by irradiation, the G2/M ratio of 4T1 cells increased to 31.14 ± 0.44 %. In contrast, 4T1 cells incubated with NGL-PEG4-FeAuNPs and PEG4-FeAuNPs showed no significant increase in the G2/M ratio, with 23.21 ± 2.40 % and 23.50 ± 1.93 %, respectively. In MDA-MB-231 cell (Figure 7 C, D), the same treatment was performed and similar results were achieved. The G2/M ratio rose from 14.31 ± 4.58 % to 26.36 ± 1.95 % as a result of 6 Gy irradiation. After being incubated with

TPP-PEG4-FeAuNPs for 24 h followed by irradiation, the G2/M ratio was 33.11 ± 1.24 %. When MDA-MB-231 cells were incubated with NGL-PEG4-FeAuNPs and PEG4-FeAuNPs before irradiation, the G2/M ratio remained at 26.44 ± 1.63 % and 24.81 ± 1.36 %, respectively. No NP-induced cell cycle arrest occurred in the absence of ionizing radiation in 4T1 and MDA-MB-231 cells. The results are consistent with the findings from the colony formation assay (Figure 6).

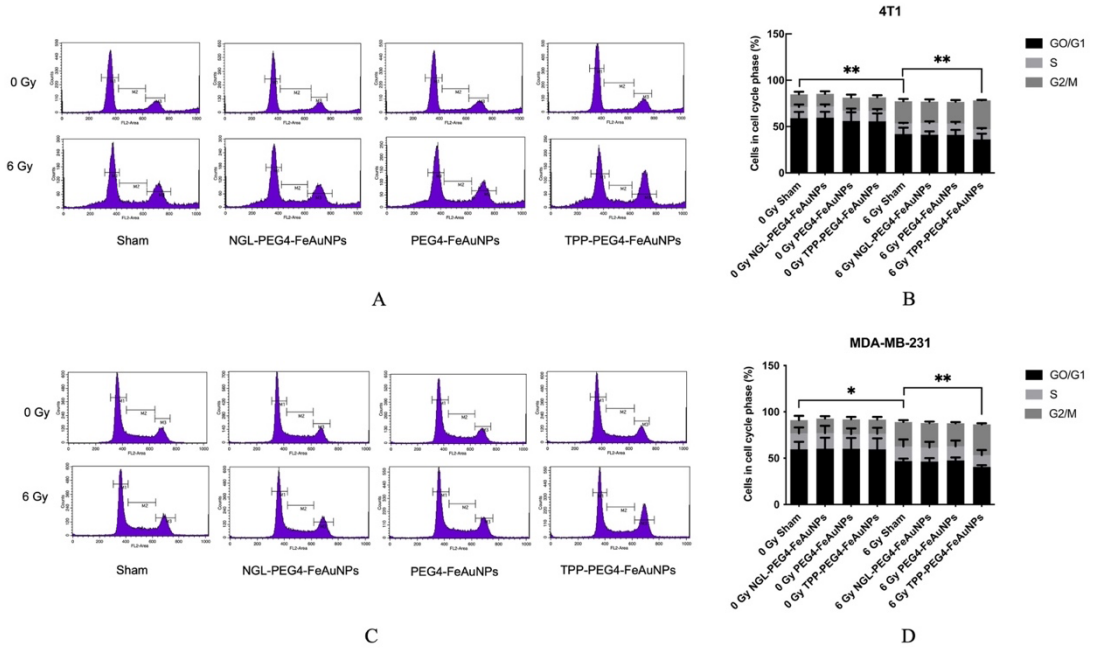

Figure 7. TPP-PEG4-FeAuNPs induce TNBC cells cell cycle arrest as a radiosensitizer. The 4T1 (A, B) and MDA-MB-231 (C, D) cells were subjected to cell cycle analysis after being exposed to NGL-PEG4-FeAuNPs, PEG4-FeAuNPs, and TPP-PEG4-FeAuNPs, each at a concentration of 2.5 μg/mL for 24 h or left untreated (sham) before being irradiated with 6 Gy. Permeabilized cells are analyzed using flow cytometry to determine the cell cycle distribution. Significance: *$p \leq 0.05$, **$p \leq 0.01$, results represent mean values ± SD of 3 independent experiments.

6.5 TPP-PEG4-FeAuNPs Induce Apoptosis in TNBCs

According to the data presented in Figure 7, TNBC cells treated with irradiation display cell cycle arrest at G2/M, and this effect is enhanced by TPP-PEG4-FeAuNPs. There is a positive correlation observed between cell cycle arrest at G2/M and apoptosis in breast cancer cells that has been exposed to irradiation (Liu et al., 2013). Next, Annexin V/PI assay by flow cytometry is used to determine the apoptosis in TNBC cells. 4T1 cells were incubated with NPs for 24 prior to irradiation. As shown in Figure 8 A, B, the 4T1 cells did not show any increase in apoptosis response when exposed to NPs (PEG4-FeAuNPs, TPP-PEG4-FeAuNPs and NGL-PEG4-FeAuNPs) only. When 4T1 cells exposed to Irradiation (6 Gy), the proportion of apoptotic cells increased to 1.39 ± 0.15-fold. A pre-incubation with NGL-PEG4-FeAuNPs and PEG4-FeAuNPs before Irradiation (6 Gy) didn't change apoptotic cells proportion, they are 1.41 ± 0.19-fold and 1.41 ± 0.21-fold, respectively. When TPP-PEG4-FeAuNPs were incubated with 4T1 cell before irradiation (6 Gy), the proportion of apoptotic cells was 2.02 ± 0.03-fold.

The Annexin V/PI assay result of MDA-MB-231 cells was shown is Figure 8 C, D. An incubation with NPs did not induce apoptosis of MDA-MB-231 cells. When MDA-MB-231 cells exposed to Irradiation (6 Gy), the proportion of apoptotic cells increased to 1.68 ± 0.31-fold. A pre-incubation with NGL-PEG4-FeAuNPs and PEG4-FeAuNPs before Irradiation (6 Gy) didn't change apoptotic cells proportion, they are 1.70 ± 0.37-fold and 1.69 ± 0.33-fold, respectively. When TPP-PEG4-FeAuNPs were incubated with MDA-MB-231 cells before irradiation (6 Gy), the proportion of apoptotic cells was

2.39 ± 0.09-fold.

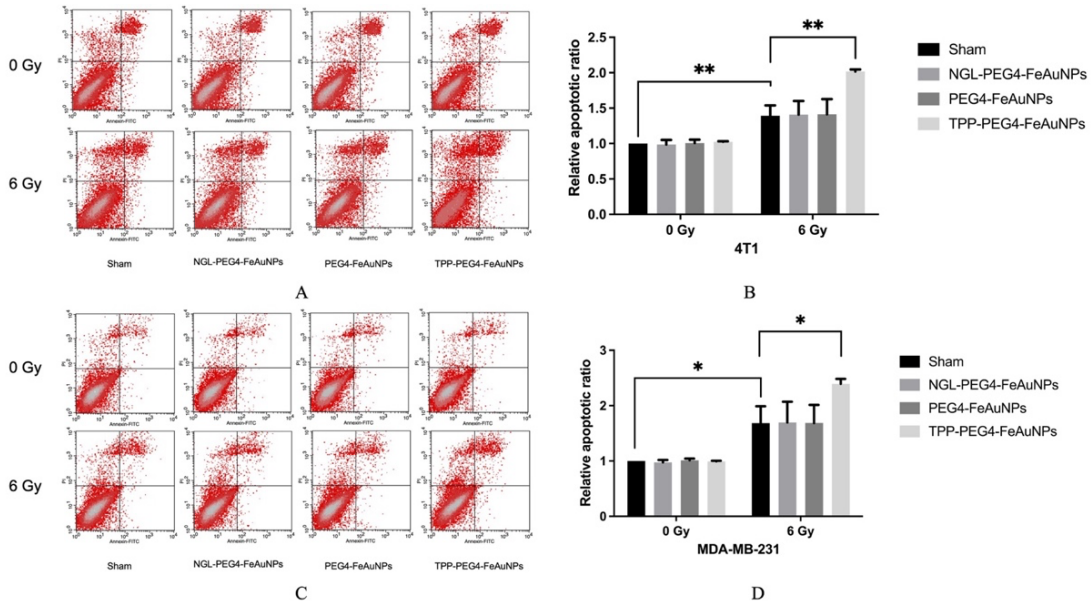

Figure 8. TPP-PEG4-FeAuNPs induce TNBC cells apoptosis as a radiosensitizer. 4T1(A, B) and MDA-MB-231 (C, D) cells were incubated with TPP-PEG4-FeAuNPs, NGL-PEG4-FeAuNPs and PEG4-FeAuNPs (2.5 μg/mL for 24 h) or sham treatment for 24h followed by an irradiation (6 Gy). Cells were analyzed for apoptosis using flow cytometry with Annexin V-FITC/PI staining. Significance: *$p \leq 0.05$, **$p \leq 0.01$; results show the mean values ± SD of 3 in-dependent experiments.

6.6 TPP-PEG4-FeAuNPs Induce Oxidative Stress in TNBCs

To investigate the oxidative stress induced by TPP-PEG4-FeAuNPs as a radiosensitizer, MDA-MB-231 cells were subjected to DCFDA staining by flow cytometry. NAC acts as a scavenger for ROS, protecting the activity of antioxidant enzymes and inhibiting the production of ROS (J. Liu et al., 2021). The proteasome inhibitor, MG132, induces cell apoptosis by increasing the production of ROS (Han,

Yang, Kim, & Park, 2010). The anti-ROS activity of NAC can be counteracted by a direct binding of MG132 to NAC (Halasi et al., 2013). The concentration of NAC used in the following experiments was 5 mM and for MG132 is 300 nM. As illustrated in Figure 9, the values of all data were standardized to the 0 Gy sham group. The ROS production increased to 1.32 ± 0.15-fold upon irradiation (6Gy) in MDA-MB-231 cells. A pre-incubation with TPP-PEG4-FeAuNPs (2.5 µg/ mL) followed by irradiation leads to an increase in ROS production to 2.48 ± 0.18-fold. When NAC was used in combination with TPP-PEG4-FeAuNPs, the ROS production was reversed (1.61 ± 0.49-fold). The highest ROS production, measuring 3.32 ± 0.23-fold, was observed when TPP-PEG4-FeAuNPs was used in combination with MG132. When MG132 was combined with NAC, the increased ROS production could be reversed and decreased to 2.50 ± 0.23-fold.

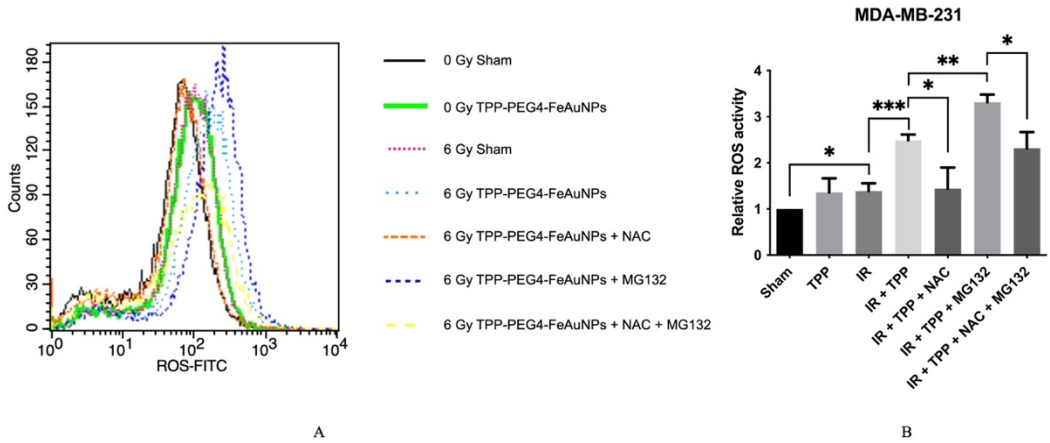

Figure 9. Analysis of the ROS production in TNBC cells. TPP-PEG4-FeAuNPs (2.5 µg/ mL), NAC (5 mM) and MG132 (300 nM) were administered alone or in combination to MDA-MB-231 cells prior to irradiation (6 Gy). 24h after irradiation, DCFDA staining was used to determine the level of ROS production by flow cytometry. Abbreviations:

IR, irradiation; TPP, TPP-PEG4-FeAuNPs; NAC, N-Acetyl-L-cysteine; MG132, Z-Leu-Leu-Leu-al. Significance: *$p \leq 0.05$, **$p \leq 0.01$, ***$p \leq 0.001$. Results represent the mean values ± SD of 3 independent experiments.

In order to explore the connection between ROS generation and the radiosensitizing effect of TPP-PEG4-FeAuNPs, MDA-MB-231 cells were subjected to the same treatments depicted in Figure 9 to assess the distribution of cell cycle and apoptosis. s shown in Figure 10 A, B, irradiation increased G2/M cell distribution from 12.05 ± 4.34 % (0Gy) to 25.00 ± 1.08 % (6 Gy). Before irradiation, a pre-incubation with TPP-PEG4-FeAuNPs for 24 h increased the ratio of cells in G2/M phase up to 33.38 ± 2.71 % (Figure 10 A, B). When NAC was used to block ROS production which is induced by TPP-PEG4-FeAuNPs, the ratio of cells in G2/M phase decreased to 23.63 ± 2.19 %. In contrast, when MG132 was used to induce ROS production, the ratio of cells in G2/M phase increased to 42.93 ± 1.50 %. When both reagents MG132 and NAC were used, the G2/M ratio was 30.22 ± 0.53 % indicating that MG132 interacts with NAC. When MDA-MB-231 cells (Figure 10 C, D) exposed to Irradiation (6 Gy), the apoptotic proportion was 2.11 ± 0.64-fold. When TPP-PEG4-FeAuNPs were incubated with MDA-MB-231 cells before irradiation (6 Gy), the apoptotic proportion was 3.30 ± 0.28-fold. When NAC was co-incubated with TPP-PEG4-FeAuNPs before irradiation (6 Gy), cell apoptotic proportion dropped to 2.07 ± 0.48-fold. When ROS production was increased by MG132 before irradiation of NP treated cells, cell apoptotic proportion reached 4.81 ± 0.59-fold. When NAC was used to bind MG132 and block its activity,

cell apoptotic proportion dropped to 2.31 ± 0.45-fold. A comparison of the ROS production (Figure 9), cell cycle arrest (Figure 10 A, B), apoptosis analysis (Figure 10 C,D) revealed that all events followed the same trend. Taken together, these findings suggest that radiosensitizing effect induced by TPP-PEG4-FeAuNPs might depend on an increased oxidative stress and a G2/M checkpoint arrest.

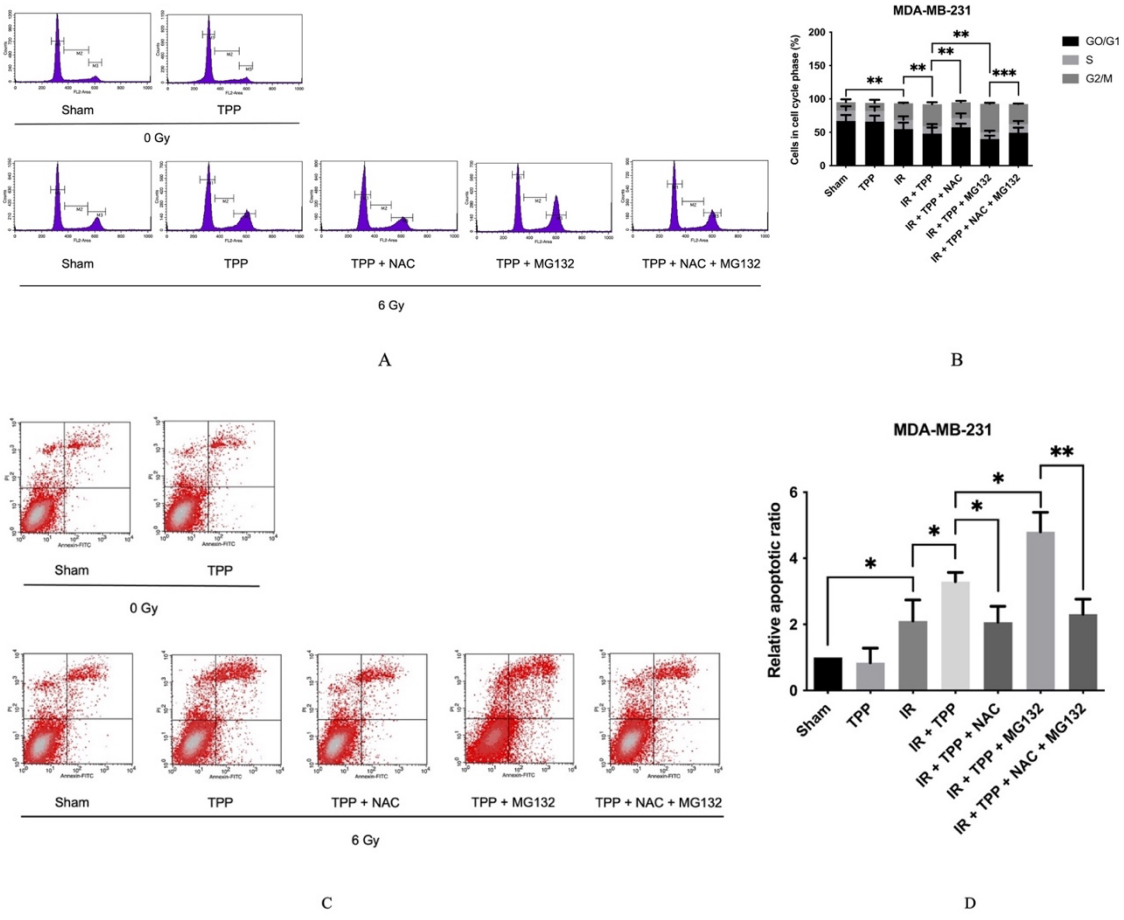

Figure 10. Cell cycle arrest and apoptosis induced by TPP-PEG4-FeAuNPs as a radiosensitizer are related with ROS production in MDA-MB-231 cells. MDA-MB-231 cells were administered with the same treatment as described in Figure 9. Cell cycle (A, B) and Annexin V-FITC/PI staining (C, D) were measured with flow cytometry. Significance: *p≤0.05, **p≤0.01, ***p≤ 0.001. Results show the mean ± SD of 3

independent experiments.

6.7 TPP-PEG4-FeAuNPs Induce DNA Double Strand Breaks in TNBCs

Ionizing irradiation is known to cause DNA double-strand breaks (Wen, Han, & Vyas, 2020). To investigate TPP-PEG4-FeAuNPs radiosensitizing effect on DNA damage, western blotting was performed to detect γ-H2AX in MDA-MB-231 cells. The treatments illustrated in Figure 11 were administered to MDA-MB-231 cells and the cells were harvest for Western blot analysis one hour after irradiation. When MDA-MB-231 cells were irradiated, γ-H2AX increased to 2.08 ± 0.26-fold. When cells were incubated with TPP-PEG4-FeAuNPs for 24h before irradiation result in a 3.11 ± 0.37-fold increase in the γ-H2AX levels. When NAC was used to block ROS production, the γ-H2AX expression was 1.52 ± 0.79-fold. When ROS production was increased by MG132 before irradiation of TPP-PEG4-FeAuNPs treated cells, the γ-H2AX levels meet the highest levels (6.24 ± 0.14-fold). When NAC was introduced to block MG132, the γ-H2AX levels dropped down to 2.55 ± 0.98-fold. In summary, the production of ROS is associated with the induction of DNA double-strand breaks by the radiosensitizing effect of TPP-PEG4-FeAuNPs

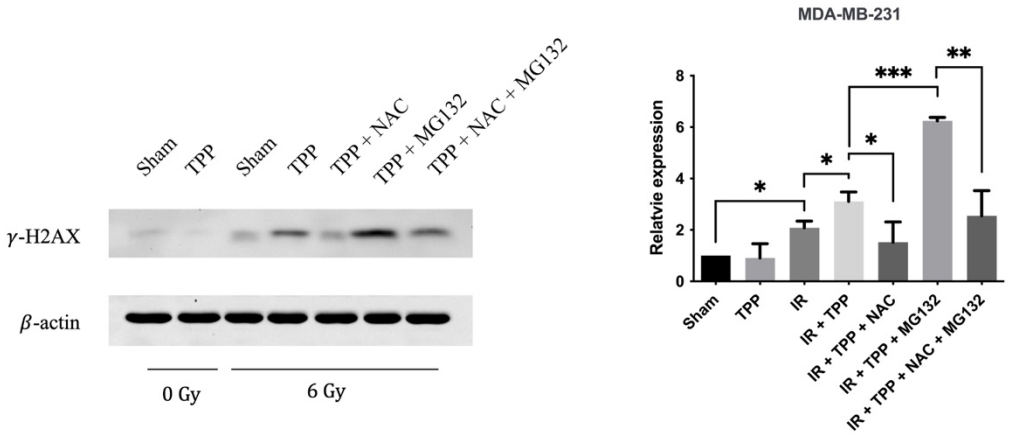

Figure 11. DNA DSBs induced by TPP-PEG4-FeAuNPs in MDA-MB-231 cells are dependent on the ROS production. MDA-MB-231 cells were subjected to treatment as described in Fig. 7. One hour after being exposed to irradiation, Cells are harvested for western blotting. γ-H2AX is used as a marker of DNA DSBs. β-actin is employed as a loading control. Significance: *$p \leq 0.05$, **$p \leq 0.01$, ***$p \leq 0.001$; results represent the mean values ± SD of 3 independent experiments.

7. Discussion

7.1 Radiotherapy on TNBC

Radiotherapy was widely used in TNBC but considering the side effects caused by off-target toxicity, its clinical effect is greatly limited(He et al., 2018). Patients with TNBC who underwent surgery followed by radiotherapy experienced significant benefits from breast cancer-specific survival and overall survival (Yao, Chu, Xu, Hu, & Song, 2019). To be precise，T3–4N1 and T1-4N2–3 stage TNBC patients achieved a better 3-year breast cancer-specific survival but not those with stage T1–2N1 (L. Zhang et al., 2020). Irradiation techniques had advanced from 2D to 3D-Conformal RT and to Intensity-Modulated Radiation Therapy (IMRT) to minimize side effects from radiotherapy (Bradley & Mendenhall, 2018). Unfortunately, side effects still exit in heart, lung, lymphoma, even secondary malignancy (Brown, Mutter, & Halyard, 2015). Cardiotoxicity is the major side effects of radiotherapy to TNBC patients. Patients were at heightened likelihood of developing coronary heart disease within the first decade of treatment and increased risk of cardiac mortality beginning in the second decade (Cheng et al., 2017).

7.2 Conjugation of TPP to hybrid FeAuNPs enhanced the cellular uptake of the nanoparticles in TNBC cells

To minimize the side effects of radiation on healthy tissues, particularly the lung and heart (Abdeltawab, Ali, Mostafa, & Hassan, 2021; Marteinsdottir et al., 2021), high-Z metal nanoparticles are used in combination with ionizing irradiation for tumor

therapies (Deng et al., 2018). Especially iron, silver, iodine and gold are frequently used for the production of high-Z metal nanoparticles (Bhattarai, Mackeyev, Venkatesulu, Krishnan, & Singh, 2021; Hainfeld, Ridwan, Stanishevskiy, & Smilowitz, 2020; Oei et al., 2019; Sears et al., 2021). AuNPs were found to improve the effectiveness of radiotherapy for squamous cell carcinoma (Hainfeld et al., 2010) and mammary carcinoma (Hainfeld, Slatkin, & Smilowitz, 2004) in mice and have a high clearance capacity through the kidneys (Hainfeld et al., 2004). To enhance nanoparticle-mediated techniques, hybrid nanoparticles were synthesized by combining the favorable biophysical properties and functions of different materials. Fe_3O_4-Au hybrid nanoparticles are widely researched due to the crucial role of the Fe_3O_4 core as a magnetic resonance imaging (MRI) contrast enhancer while the gold shell has the ability to act as a radiosensitizer through the emission of secondary Auger electrons (Efremova et al., 2018). Improving the targeting capability of nanoparticles can be achieved by linking agents that can target tumors, such as peptides or antibodies. Nanoparticles functionalized with human mesenchymal stem cells (Pullambhatla et al., 2020), peptide (Vilchis-Juarez et al., 2014) and antibody (Lu et al., 2021) demonstrated a strong attraction to tumors in mice. The current study employed TPP, a 14-mer peptide, to specifically target highly aggressive TNBC cells that express mHsp70. The conjugation of TPP to FeAuNPs facilitated a better uptake by TNBC cells. After NPs entered the cells, the distribution of NPs around the tumor cell nucleus was more homogenous. Absence of mHsp70 expression in normal cells reduced their likelihood of internalizing TPP-functionalized nanoparticles. TPP peptide exhibits a

notable tendency to self-aggregate, likely due to its similarity in sequence to the Hsp70 oligomerization domain (Stangl, Tei, et al., 2018). To enhance the stability, solubility, and distribution rate of hybrid nanoparticles, PEG, a 4-mer chain, was introduced into the TPP moiety with binding activity to avoid its self-aggregation(Francis, Delgado, Fisher, Malik, & Agrawal, 1996; Hamidi et al., 2008). FeAuNPs that have been functionalized with TPP have a diameter of 4 nm in this study. Study showed that the efficiency of NPs penetrating the nucleus is related to its size, with smaller NPs having a higher effectiveness (Fan et al., 2020). Another two hybrid FeAuNPs were developed as internal controls, one with PEG4 linker and a 14-mer nonspecific peptide (NGL-PEG4-FeAuNPs) and another with PEG4 linker but not any peptide (PEG4-FeAuNPs).

7.3 TNBC cells with high mHsp70 expression

The expression of mHsp70 on cells determined whether TPP functionalized hybrid nanoparticles can be taken up by cells. The membrane Hsp70 status of TNBC cells 4T1 and MDA-MB-231 were checked before treating TNBC with hybrid nanoparticles. As expected, both 4T1 and MDA-MB-231, which are highly aggressive tumor cells, showed strong mHsp70 expression, making them eligible for Hsp70 target therapy. In contrast to TNBC cells, the expression of mHsp70 in normal cell PBL was very low. In previous studies, Hsp70-targeting probes like TPP peptide (Stangl, Tei, et al., 2018) and cmHsp70.1 antibody (Stangl, Gehrmann, Dressel, et al., 2011) showed rapid internalization into tumor cells with mHsp70-positive. Compared with control NPs, AuNPs functionalized with cmHsp70.1 antibody showed a significant enrichment in

tumor cells (Kimm et al., 2020).

7.4 mHsp70-targeting peptide TPP increase tumor affinity and radiosensitizing effects of FeAuNPs

When MDA-MB-231 cells were incubated with different NP formulations, only TPP-PEG4-FeAuNPs demonstrated a significant increase in enrichment within MDA-MB-231 cells. But the relationship between Hsp70 membrane status and tumor affinity to TPP was remained unclear. So, the mHsp70 negative normal cells (PBL) were used in the further experiments. Whereas neither TPP-PEG4-FeAuNPs nor NGL-PEG4-FeAuNPs showed enrichment in PBL. Among different NP formulations, TPP-PEG4-FeAuNPs are more homogeneously distributed around the nucleus of MDA-MB-231 cells. The targeting of AuNPs to the nucleus of tumor cells markedly increases their sensitivity to radiation. Previous study showed AuNPs target the tumor cells nucleus and significantly enhance their radiosensitivity (Ozcelik & Pratx, 2020) due to the Auger electrons' short range (2–500 nm) (Kassis & Adelstein, 2005). Proximity of TPP-PEG4-FeAuNPs to the nucleus is crucial for inducing DNA damage in tumor cells following irradiation. The initial evaluation of whether TPP-PEG4-FeAuNPs exhibit radiosensitizing effects involved testing them in a colony formation assay. In both 4T1 and MDA-MB-231 cells, the clonogenic cell survival decreased in a manner that depended on the irradiation dose. While pre-treatment with TPP-PEG4-FeAuNPs significantly enhanced the ability to kill tumor cells upon irradiation, treatment with NGL-PEG4-FeAuNPs and PEG4-FeAuNPs did not demonstrate any significant effects. The colony formation assays demonstrate that the mHsp70-targeting peptide TPP

improved the affinity and uptake of FeAuNPs, and FeAuNPs also increased the radiosensitivity of TNBC cells.

7.5 TPP functionalized FeAuNPs induce G2/M cell cycle arrest and apoptosis followed by irradiation.

G2/M arrest following irradiation is essential for tumor cells to prevent mitosis in DNA-damaged cells (Peng et al., 2020). In breast cancer cells, miR-21 expression compromised cell cycle progression to induce radiation resistance (Anastasov et al., 2012). In previous study, radiation induces TNBC cells 4T1 and MDA-MB-231 was confirmed that cell cycle arrest occurred at the radiosensitive G2/M phase (Masoudi-Khoram et al., 2020). In this study, cell cycle analysis by flow cytometer was used for the G2/M checkpoint arrest study. 4T1 and MDA-MB-231 cells were culture with or without different formations of FeAuNPs followed with irradiation. A single irradiation (6 Gy) induced G2/M arrest as expected in both cell lines. The combination of TPP-PEG4-FeAuNPs, but not other formations of FeAuNPs, with irradiation resulted in a more pronounced G2/M arrest compared to irradiation alone. The G2/M arrest increased NPs internalization efficiency (Kim, Aberg, Salvati, & Dawson, 2011) and nuclear uptake (L. Li, Sun, Zhang, & Huang, 2016). Cell cycle distribution is closely related to apoptosis, disruption of the cell cycle is a powerful inducer of apoptosis(Evan, Brown, Whyte, & Harrington, 1995). The phosphorylated anti-apoptotic Bcl-2 protein was observed in G2/M phase but not in other cell cycle phases(L. Li, Yang, Wang, & Kopecek, 2019). The findings of this study were validated in cells of both 4T1 and MDA-MB-231, thus confirming the previously reported result. The proportion of

apoptotic cells is highest in TNBCs treated with TPP-PEG4-FeAuNPs followed by irradiation. Other formations of FeAuNPs showed no significant impact on cell apoptosis followed by irradiation.

7.6 TPP-PEG4-FeAuNPs radiosensitizing effect is related with an increased ROS production

ROS are constantly produced within the mitochondria through the process of electron transport chain(Zhao, Jiang, Zhang, & Yu, 2019). It has a crucial role in multiple signaling pathways, such as cell cycle arrest and apoptosis (Kuczler, Olseen, Pienta, & Amend, 2021; F. Wang et al., 2021). Irradiation can increase ROS production in various types of cancer cells (Hasegawa et al., 2020; Z. Zhang, Lu, et al., 2021). ROS production induced by irradiation occurs through the sensing of Ca2+ channels is associated with a dysfunction in the salivary gland in mice (Liu, Subedi, Zheng, & Ambudkar, 2021). DCFDA/H_2DCFDA staining was chose to determine ROS production level in this study. DCFDA/H2DCFDA serves as a general indicator of various types of ROS, rather than a specific detector for a certain ROS type (Setsukinai, Urano, Kakinuma, Majima, & Nagano, 2003). My experiments showed that irradiation leads to a rise of ROS production in TNBC cells. The exposure to irradiation (6 Gy) triggered the generation of ROS, and the co-treatment with TPP-PEG4-FeAuNPs led to a greater increase in ROS production compared to irradiation alone. To explore the link between the radiosensitizing effect and ROS production, the ROS inhibitor NAC was applied. In MDA-MB-231 cells, the findings demonstrated that NAC suppressed the generation of ROS triggered by both irradiation and TPP-PEG4-FeAuNPs. In the

further study, the relationship between ROS and cell apoptosis was explored. The results indicated a consistent pattern between the increase in ROS production and apoptosis. Furthermore, inhibition of ROS also led to a decrease in apoptosis. The occurrence of cell apoptosis is reliant on the arrest of G2/M cell cycle and elevated ROS generation.

7.7 DNA double strands breaks related with ROS production

DNA double strand breaks are strongly associated with high levels of ROS produced by irradiation (Yalcin et al., 2022). In Qin's study, biogenetic gold nanoparticles followed by irradiation strengthened the ROS generation and DNA damage(Qin et al., 2021). γ-H2AX is one of the most reliable markers of DNA DSBs (Wanotayan et al., 2022). The relationship between elevated levels of ROS and an increase in frequency of DNA DSBs, as evidenced by higher expression of γ-H2AX, was demonstrated using Western blot. The results showed that in MDA-MB-231 cells, an increased γ-H2AX expression follow by irradiation and pre-treatment with TPP-PEG4-AuNPs was closely associated with elevated ROS production. The effect of DNA damage was intensified by the addition of the proteasome inhibitor MG132, but completely mitigated by NAC. The effectiveness of irradiation in anticancer was not compromised by the presence of NAC, which prevented ROS in MDA-MB-231 cells(H. Wang & Zhang, 2019). The Auger electrons emitted by AuNPs under X-ray exposure have a limited effective range of 2-500nm (Kassis & Adelstein, 2005). Therefore, the accumulation of TPP-PEG4-FeAuNPs adjacent to the nucleus in tumor cells was shown to enhance radiosensitivity.

However, the mechanism by which the TPP peptide assists in the transport of NPs to the tumor cell nucleus remains to be elucidated.

8. Conclusion

In my study, the radiosensitizing effect of the novel Fe3O4-Au nanoparticles functionalized with the TPP peptide targeting mHsp70-positive TNBCs is investigated. TPP peptide boosted the affinity and uptake of Fe_3O_4-Au hybrid nanoparticles by TNBCs. TPP-PEG4-FeAuNPs, unlike the control hybrid FeAuNPs, remarkably enhance the radiosensitivity of TNBCs by inducing a G2/M checkpoint arrest, producing more ROS, and thus causing DNA damage. The DNA damage has been found to depend on the increased ROS production. Further *in vivo* studies are necessary to explore the effects of TPP functionalized hybrid FeAuNPs in mouse models to study their radiosensitizing effect *in vivo*.

9. Reference

Abdeltawab, A. A., Ali, S. A., Mostafa, H. G., & Hassan, M. A. (2021). Predictive Factors Increasing the Risk of Radiation Toxicity in Patients with Early Breast Cancer. *Asian Pac J Cancer Prev, 22*(1), 145-149. doi:10.31557/APJCP.2021.22.1.145

Akasaka, M., Nishi, T., & Niidome, Y. (2021). Gold-Silver and Gold-Palladium Alloy Nanoparticles as Mass-Probes for Immunosensing. *Anal Sci, 37*(9), 1305-1307. doi:10.2116/analsci.21N001

Anastasov, N., Hofig, I., Vasconcellos, I. G., Rappl, K., Braselmann, H., Ludyga, N., . . . Atkinson, M. J. (2012). Radiation resistance due to high expression of miR-21 and G2/M checkpoint arrest in breast cancer cells. *Radiat Oncol, 7*, 206. doi:10.1186/1748-717X-7-206

Bardia, A., Hurvitz, S. A., Tolaney, S. M., Loirat, D., Punie, K., Oliveira, M., . . . Investigators, A. C. T. (2021). Sacituzumab Govitecan in Metastatic Triple-Negative Breast Cancer. *N Engl J Med, 384*(16), 1529-1541. doi:10.1056/NEJMoa2028485

Bareche, Y., Buisseret, L., Gruosso, T., Girard, E., Venet, D., Dupont, F., . . . Sotiriou, C. (2020). Unraveling Triple-Negative Breast Cancer Tumor Microenvironment Heterogeneity: Towards an Optimized Treatment Approach. *J Natl Cancer Inst, 112*(7), 708-719. doi:10.1093/jnci/djz208

Bashiri Dezfouli, A., Yazdi, M., Pockley, A. G., Khosravi, M., Kobold, S., Wagner, E., & Multhoff, G. (2021). NK cells armed with chimeric antigen receptors (CAR): Roadblocks to successful development. *Cells, 10*(12), 3390.

Bhagat, S., Srikanth Vallabani, N. V., Shutthanandan, V., Bowden, M., Karakoti, A. S., & Singh, S. (2018). Gold core/ceria shell-based redox active nanozyme mimicking the biological multienzyme complex phenomenon. *J Colloid Interface Sci, 513*, 831-842. doi:10.1016/j.jcis.2017.11.064

Bhattarai, S., Mackeyev, Y., Venkatesulu, B. P., Krishnan, S., & Singh, P. K. (2021). CXC chemokine receptor 4 (CXCR4) targeted gold nanoparticles potently enhance radiotherapy outcomes in breast cancer. *Nanoscale, 13*(45), 19056-19065. doi:10.1039/d1nr05385j

Bothou, A., Zervoudis, S., Iliadou, M., Pappou, P., Iatrakis, G., Tsatsaris, G., . . . Tsikouras, P. (2022). Breastfeeding and Breast Cancer Risk: Our Experience and Mini-review of the Literature. *Mater Sociomed, 34*(1), 28-32. doi:10.5455/msm.2022.33.28-32

Bradley, J. A., & Mendenhall, N. P. (2018). Novel Radiotherapy Techniques for Breast Cancer. *Annu Rev Med, 69*, 277-288. doi:10.1146/annurev-med-042716-103422

Brown, L. C., Mutter, R. W., & Halyard, M. Y. (2015). Benefits, risks, and safety of external beam radiation therapy for breast cancer. *Int J Womens Health, 7*, 449-458. doi:10.2147/IJWH.S55552

Cai, J., Miao, Y. Q., Li, L., & Fan, H. M. (2018). Facile Preparation of Gold-Decorated Fe(3)O(4) Nanoparticles for CT and MR Dual-Modal Imaging. *Int J Mol Sci,*

19(12). doi:10.3390/ijms19124049

Chen, F., Wen, W., Long, J., Shu, X., Yang, Y., Shu, X. O., & Zheng, W. (2022). Mendelian randomization analyses of 23 known and suspected risk factors and biomarkers for breast cancer overall and by molecular subtypes. *Int J Cancer, 151*(3), 372-380. doi:10.1002/ijc.34026

Chen, R., Sun, Y., Huo, B., Mao, Z., Wang, X., Li, S., . . . Gao, Z. (2021). Development of Fe3O4@Au nanoparticles coupled to Au@Ag core-shell nanoparticles for the sensitive detection of zearalenone. *Anal Chim Acta, 1180*, 338888. doi:10.1016/j.aca.2021.338888

Cheng, Y. J., Nie, X. Y., Ji, C. C., Lin, X. X., Liu, L. J., Chen, X. M., . . . Wu, S. H. (2017). Long-Term Cardiovascular Risk After Radiotherapy in Women With Breast Cancer. *J Am Heart Assoc, 6*(5). doi:10.1161/JAHA.117.005633

Colvin, T. A., Gabai, V. L., Gong, J., Calderwood, S. K., Li, H., Gummuluru, S., . . . Sherman, M. Y. (2014). Hsp70-Bag3 interactions regulate cancer-related signaling networks. *Cancer Res, 74*(17), 4731-4740. doi:10.1158/0008-5472.CAN-14-0747

Deng, J., Xu, S., Hu, W., Xun, X., Zheng, L., & Su, M. (2018). Tumor targeted, stealthy and degradable bismuth nanoparticles for enhanced X-ray radiation therapy of breast cancer. *Biomaterials, 154*, 24-33. doi:10.1016/j.biomaterials.2017.10.048

Dezfouli, A. B., Yazdi, M., Benmebarek, M.-R., Schwab, M., Michaelides, S., Miccichè, A., . . . Wagner, E. (2022). CAR T cells targeting membrane-bound Hsp70 on tumor cells mimic Hsp70-primed NK cells. *Frontiers in Immunology, 13*.

Durand, M., Lelievre, E., Chateau, A., Berquand, A., Laurent, G., Carl, P., . . . Pinel, S. (2021). The detrimental invasiveness of glioma cells controlled by gadolinium chelate-coated gold nanoparticles. *Nanoscale, 13*(20), 9236-9251. doi:10.1039/d0nr08936b

Efremova, M. V., Naumenko, V. A., Spasova, M., Garanina, A. S., Abakumov, M. A., Blokhina, A. D., . . . Wiedwald, U. (2018). Magnetite-Gold nanohybrids as ideal all-in-one platforms for theranostics. *Sci Rep, 8*(1), 11295. doi:10.1038/s41598-018-29618-w

Enea, M., Pereira, E., Costa, J., Soares, M. E., Dias da Silva, D., Bastos, M. L., & Carmo, H. F. (2021). Cellular uptake and toxicity of gold nanoparticles on two distinct hepatic cell models. *Toxicol In Vitro, 70*, 105046. doi:10.1016/j.tiv.2020.105046

Erickson, B. K., Zeybek, B., Santin, A. D., & Fader, A. N. (2020). Targeting human epidermal growth factor receptor 2 (HER2) in gynecologic malignancies. *Curr Opin Obstet Gynecol, 32*(1), 57-64. doi:10.1097/GCO.0000000000000599

Evan, G. I., Brown, L., Whyte, M., & Harrington, E. (1995). Apoptosis and the cell cycle. *Curr Opin Cell Biol, 7*(6), 825-834. doi:10.1016/0955-0674(95)80066-2

Fan, M., Han, Y., Gao, S., Yan, H., Cao, L., Li, Z., . . . Zhang, J. (2020). Ultrasmall gold nanoparticles in cancer diagnosis and therapy. *Theranostics, 10*(11), 4944-4957. doi:10.7150/thno.42471

Feng, W., Zhou, X., Nie, W., Chen, L., Qiu, K., Zhang, Y., & He, C. (2015).

Au/polypyrrole@Fe3O4 nanocomposites for MR/CT dual-modal imaging guided-photothermal therapy: an in vitro study. *ACS Appl Mater Interfaces, 7*(7), 4354-4367. doi:10.1021/am508837v

Francis, G. E., Delgado, C., Fisher, D., Malik, F., & Agrawal, A. K. (1996). Polyethylene glycol modification: relevance of improved methodology to tumour targeting. *J Drug Target, 3*(5), 321-340. doi:10.3109/10611869608996824

Garnica-Garza, H. M. (2013). Microdosimetry of X-ray-irradiated gold nanoparticles. *Radiat Prot Dosimetry, 155*(1), 59-63. doi:10.1093/rpd/ncs278

Gehrmann, M., Specht, H. M., Bayer, C., Brandstetter, M., Chizzali, B., Duma, M., . . . Multhoff, G. (2014). Hsp70--a biomarker for tumor detection and monitoring of outcome of radiation therapy in patients with squamous cell carcinoma of the head and neck. *Radiat Oncol, 9*, 131. doi:10.1186/1748-717X-9-131

Giri, B., Sharma, P., Jain, T., Ferrantella, A., Vaish, U., Mehra, S., . . . Dudeja, V. (2021). Hsp70 modulates immune response in pancreatic cancer through dendritic cells. *Oncoimmunology, 10*(1), 1976952. doi:10.1080/2162402X.2021.1976952

Hainfeld, J. F., Dilmanian, F. A., Zhong, Z., Slatkin, D. N., Kalef-Ezra, J. A., & Smilowitz, H. M. (2010). Gold nanoparticles enhance the radiation therapy of a murine squamous cell carcinoma. *Phys Med Biol, 55*(11), 3045-3059. doi:10.1088/0031-9155/55/11/004

Hainfeld, J. F., Ridwan, S. M., Stanishevskiy, F. Y., & Smilowitz, H. M. (2020). Iodine nanoparticle radiotherapy of human breast cancer growing in the brains of athymic mice. *Sci Rep, 10*(1), 15627. doi:10.1038/s41598-020-72268-0

Hainfeld, J. F., Slatkin, D. N., & Smilowitz, H. M. (2004). The use of gold nanoparticles to enhance radiotherapy in mice. *Phys Med Biol, 49*(18), N309-315. doi:10.1088/0031-9155/49/18/n03

Halasi, M., Wang, M., Chavan, T. S., Gaponenko, V., Hay, N., & Gartel, A. L. (2013). ROS inhibitor N-acetyl-L-cysteine antagonizes the activity of proteasome inhibitors. *Biochem J, 454*(2), 201-208. doi:10.1042/BJ20130282

Hamidi, M., Rafiei, P., & Azadi, A. (2008). Designing PEGylated therapeutic molecules: advantages in ADMET properties. *Expert Opin Drug Discov, 3*(11), 1293-1307. doi:10.1517/17460441.3.11.1293

Han, Y. H., Yang, Y. M., Kim, S. Z., & Park, W. H. (2010). Attenuation of MG132-induced HeLa cell death by N-acetyl cysteine via reducing reactive oxygen species and preventing glutathione depletion. *Anticancer Res, 30*(6), 2107-2112. Retrieved from https://www.ncbi.nlm.nih.gov/pubmed/20651358

Hasegawa, T., Takahashi, J., Nagasawa, S., Doi, M., Moriyama, A., & Iwahashi, H. (2020). DNA Strand Break Properties of Protoporphyrin IX by X-Ray Irradiation against Melanoma. *Int J Mol Sci, 21*(7). doi:10.3390/ijms21072302

Hassanen, E. I., Korany, R. M. S., & Bakeer, A. M. (2021). Cisplatin-conjugated gold nanoparticles-based drug delivery system for targeting hepatic tumors. *J Biochem Mol Toxicol, 35*(5), e22722. doi:10.1002/jbt.22722

He, M. Y., Rancoule, C., Rehailia-Blanchard, A., Espenel, S., Trone, J. C., Bernichon, E., . . . Magne, N. (2018). Radiotherapy in triple-negative breast cancer: Current

situation and upcoming strategies. *Crit Rev Oncol Hematol, 131*, 96-101. doi:10.1016/j.critrevonc.2018.09.004

Huwaidi, A., Kumari, B., Robert, G., Guerin, B., Sanche, L., & Wagner, J. R. (2021). Profiling DNA Damage Induced by the Irradiation of DNA with Gold Nanoparticles. *J Phys Chem Lett, 12*(40), 9947-9954. doi:10.1021/acs.jpclett.1c02598

Jin, T., Wang, X., Deng, Z., Liu, X., & Liang, D. (2021). ROS-induced dramatic lipid changes in Arabidopsis. *Redox Rep, 26*(1), 190-196. doi:10.1080/13510002.2021.2002001

Kabakov, A. E., & Gabai, V. L. (2021). HSP70s in Breast Cancer: Promoters of Tumorigenesis and Potential Targets/Tools for Therapy. *Cells, 10*(12). doi:10.3390/cells10123446

Kang, N., Xu, D., Han, Y., Lv, X., Chen, Z., Zhou, T., . . . Zhou, X. (2019). Magnetic targeting core/shell Fe3O4/Au nanoparticles for magnetic resonance/photoacoustic dual-modal imaging. *Mater Sci Eng C Mater Biol Appl, 98*, 545-549. doi:10.1016/j.msec.2019.01.013

Kassis, A. I., & Adelstein, S. J. (2005). Radiobiologic principles in radionuclide therapy. *J Nucl Med, 46 Suppl 1*, 4S-12S. Retrieved from https://www.ncbi.nlm.nih.gov/pubmed/15653646

Katifelis, H., Lyberopoulou, A., Vityuk, N., Grammatikaki, M., Pylypchuk, I., Lazaris, F., . . . Gazouli, M. (2020). In vitro effect of hyperthermic Ag and Au Fe3O4 nanoparticles in cancer cells. *J BUON, 25*(2), 1212-1218. Retrieved from https://www.ncbi.nlm.nih.gov/pubmed/32521928

Kim, J. A., Aberg, C., Salvati, A., & Dawson, K. A. (2011). Role of cell cycle on the cellular uptake and dilution of nanoparticles in a cell population. *Nat Nanotechnol, 7*(1), 62-68. doi:10.1038/nnano.2011.191

Kimm, M. A., Shevtsov, M., Werner, C., Sievert, W., Zhiyuan, W., Schoppe, O., . . . Stangl, S. (2020). Gold Nanoparticle Mediated Multi-Modal CT Imaging of Hsp70 Membrane-Positive Tumors. *Cancers (Basel), 12*(5). doi:10.3390/cancers12051331

Ku, A., Facca, V. J., Cai, Z., & Reilly, R. M. (2019). Auger electrons for cancer therapy - a review. *EJNMMI Radiopharm Chem, 4*(1), 27. doi:10.1186/s41181-019-0075-2

Kuczler, M. D., Olseen, A. M., Pienta, K. J., & Amend, S. R. (2021). ROS-induced cell cycle arrest as a mechanism of resistance in polyaneuploid cancer cells (PACCs). *Prog Biophys Mol Biol, 165*, 3-7. doi:10.1016/j.pbiomolbio.2021.05.002

Kuncic, Z., & Lacombe, S. (2018). Nanoparticle radio-enhancement: principles, progress and application to cancer treatment. *Phys Med Biol, 63*(2), 02TR01. doi:10.1088/1361-6560/aa99ce

Li, L., Lv, D., Zhai, J., Zhang, D., Guan, X., & Ma, F. (2021). Breast Cancer in Chinese Females Aged 25 Years and Younger. *J Oncol, 2021*, 4891936. doi:10.1155/2021/4891936

Li, L., Sun, W., Zhang, Z., & Huang, Y. (2016). Time-staggered delivery of docetaxel

and H1-S6A,F8A peptide for sequential dual-strike chemotherapy through tumor priming and nuclear targeting. *J Control Release, 232*, 62-74. doi:10.1016/j.jconrel.2016.04.021

Li, L., Yang, J., Wang, J., & Kopecek, J. (2019). Drug-free macromolecular therapeutics exhibit amplified apoptosis in G2/M phase arrested cells. *J Drug Target, 27*(5-6), 566-572. doi:10.1080/1061186X.2018.1521414

Li, X., Fang, X., Li, S., Lui, K. H., Lo, W. S., Gu, Y., & Wong, W. T. (2021). Nitroreductase-Induced Aggregation of Gold Nanoparticles for "Off-On" Photoacoustic Imaging of Tumor Hypoxia. *J Biomed Nanotechnol, 17*(11), 2186-2197. doi:10.1166/jbn.2021.3195

Li, X., Yang, J., Peng, L., Sahin, A. A., Huo, L., Ward, K. C., . . . Meisel, J. L. (2017). Triple-negative breast cancer has worse overall survival and cause-specific survival than non-triple-negative breast cancer. *Breast Cancer Res Treat, 161*(2), 279-287. doi:10.1007/s10549-016-4059-6

Lin, N. U., Claus, E., Sohl, J., Razzak, A. R., Arnaout, A., & Winer, E. P. (2008). Sites of distant recurrence and clinical outcomes in patients with metastatic triple-negative breast cancer: high incidence of central nervous system metastases. *Cancer, 113*(10), 2638-2645. doi:10.1002/cncr.23930

Liu, J., Liu, Q., Han, J., Feng, J., Guo, T., Li, Z., . . . Peng, X. (2021). N-Acetylcysteine Inhibits Patulin-Induced Apoptosis by Affecting ROS-Mediated Oxidative Damage Pathway. *Toxins (Basel), 13*(9). doi:10.3390/toxins13090595

Liu, X., Subedi, K. P., Zheng, C., & Ambudkar, I. (2021). Mitochondria-targeted antioxidant protects against irradiation-induced salivary gland hypofunction. *Sci Rep, 11*(1), 7690. doi:10.1038/s41598-021-86927-3

Liu, X., Sun, C., Jin, X., Li, P., Ye, F., Zhao, T., . . . Li, Q. (2013). Genistein enhances the radiosensitivity of breast cancer cells via G(2)/M cell cycle arrest and apoptosis. *Molecules, 18*(11), 13200-13217. doi:10.3390/molecules181113200

Lu, Y., Huang, J., Li, F., Wang, Y., Ding, M., Zhang, J., . . . Ren, X. (2021). EGFR-specific single-chain variable fragment antibody-conjugated Fe3O4/Au nanoparticles as an active MRI contrast agent for NSCLC. *MAGMA, 34*(4), 581-591. doi:10.1007/s10334-021-00916-1

Marteinsdottir, M., Wang, C. C., McNamara, A., Depauw, N., Shin, J., & Paganetti, H. (2021). The impact of variable relative biological effectiveness in proton therapy for left-sided breast cancer when estimating normal tissue complications in the heart and lung. *Phys Med Biol, 66*(3), 035023. doi:10.1088/1361-6560/abd230

Mashat, R. M., Zielinska, H. A., Holly, J. M. P., & Perks, C. M. (2021). A Role for ER-Beta in the Effects of Low-Density Lipoprotein Cholesterol and 27-Hydroxycholesterol on Breast Cancer Progression: Involvement of the IGF Signalling Pathway? *Cells, 11*(1). doi:10.3390/cells11010094

Masoudi-Khoram, N., Abdolmaleki, P., Hosseinkhan, N., Nikoofar, A., Mowla, S. J., Monfared, H., & Baldassarre, G. (2020). Differential miRNAs expression pattern of irradiated breast cancer cell lines is correlated with radiation sensitivity. *Sci Rep, 10*(1), 9054. doi:10.1038/s41598-020-65680-z

Mawson, A., Lai, A., Carroll, J. S., Sergio, C. M., Mitchell, C. J., & Sarcevic, B. (2005).

Estrogen and insulin/IGF-1 cooperatively stimulate cell cycle progression in MCF-7 breast cancer cells through differential regulation of c-Myc and cyclin D1. *Mol Cell Endocrinol, 229*(1-2), 161-173. doi:10.1016/j.mce.2004.08.002

Miller, K. D., Fidler-Benaoudia, M., Keegan, T. H., Hipp, H. S., Jemal, A., & Siegel, R. L. (2020). Cancer statistics for adolescents and young adults, 2020. *CA Cancer J Clin, 70*(6), 443-459. doi:10.3322/caac.21637

Multhoff, G., Botzler, C., Wiesnet, M., Muller, E., Meier, T., Wilmanns, W., & Issels, R. D. (1995). A stress-inducible 72-kDa heat-shock protein (HSP72) is expressed on the surface of human tumor cells, but not on normal cells. *Int J Cancer, 61*(2), 272-279. doi:10.1002/ijc.2910610222

Ngwa, W., Makrigiorgos, G. M., & Berbeco, R. I. (2012). Gold nanoparticle-aided brachytherapy with vascular dose painting: estimation of dose enhancement to the tumor endothelial cell nucleus. *Med Phys, 39*(1), 392-398. doi:10.1118/1.3671905

Oei, A. L., Korangath, P., Mulka, K., Helenius, M., Coulter, J. B., Stewart, J., . . . Ivkov, R. (2019). Enhancing the abscopal effect of radiation and immune checkpoint inhibitor therapies with magnetic nanoparticle hyperthermia in a model of metastatic breast cancer. *Int J Hyperthermia, 36*(sup1), 47-63. doi:10.1080/02656736.2019.1685686

Oumano, M., Russell, L., Salehjahromi, M., Shanshan, L., Sinha, N., Ngwa, W., & Yu, H. (2021). CT imaging of gold nanoparticles in a human-sized phantom. *J Appl Clin Med Phys, 22*(1), 337-342. doi:10.1002/acm2.13155

Ozcelik, S., & Pratx, G. (2020). Nuclear-targeted gold nanoparticles enhance cancer cell radiosensitization. *Nanotechnology, 31*(41), 415102. doi:10.1088/1361-6528/aba02b

Park, S. L., Chung, T. W., Kim, S., Hwang, B., Kim, J. M., Lee, H. M., . . . Moon, S. K. (2017). HSP70-1 is required for interleukin-5-induced angiogenic responses through eNOS pathway. *Sci Rep, 7*, 44687. doi:10.1038/srep44687

Peng, Y., Fu, S., Hu, W., Qiu, Y., Zhang, L., Tan, R., & Sun, L. Q. (2020). Glutamine synthetase facilitates cancer cells to recover from irradiation-induced G2/M arrest. *Cancer Biol Ther, 21*(1), 43-51. doi:10.1080/15384047.2019.1665394

Pullambhatla, M., Rowe, S. P., Lisok, A., Wang, Y., Todd, G. P., Danilkovitch, A., & Pomper, M. G. (2020). Enhancement of Radiotherapy with Human Mesenchymal Stem Cells Containing Gold Nanoparticles. *Tomography, 6*(4), 373-378. doi:10.18383/j.tom.2020.00026

Qin, X., Yang, C., Xu, H., Zhang, R., Zhang, D., Tu, J., . . . Zhang, Z. (2021). Cell-Derived Biogenetic Gold Nanoparticles for Sensitizing Radiotherapy and Boosting Immune Response against Cancer. *Small, 17*(50), e2103984. doi:10.1002/smll.202103984

Qiu, J., Zhang, T., Zhu, X., Yang, C., Wang, Y., Zhou, N., . . . Qiu, C. (2019). Hyperoside Induces Breast Cancer Cells Apoptosis via ROS-Mediated NF-kappaB Signaling Pathway. *Int J Mol Sci, 21*(1). doi:10.3390/ijms21010131

Qiu, R., Zhong, Y., Hu, M., & Wu, B. (2022). Breastfeeding and Reduced Risk of Breast Cancer: A Systematic Review and Meta-Analysis. *Comput Math Methods Med,*

2022, 8500910. doi:10.1155/2022/8500910

Reczek, C. R., Birsoy, K., Kong, H., Martinez-Reyes, I., Wang, T., Gao, P., . . . Chandel, N. S. (2017). A CRISPR screen identifies a pathway required for paraquat-induced cell death. *Nat Chem Biol, 13*(12), 1274-1279. doi:10.1038/nchembio.2499

Riley, P. A. (1994). Free radicals in biology: oxidative stress and the effects of ionizing radiation. *Int J Radiat Biol, 65*(1), 27-33. doi:10.1080/09553009414550041

Sears, J., Swanner, J., Fahrenholtz, C. D., Snyder, C., Rohde, M., Levi-Polyachenko, N., & Singh, R. (2021). Combined Photothermal and Ionizing Radiation Sensitization of Triple-Negative Breast Cancer Using Triangular Silver Nanoparticles. *Int J Nanomedicine, 16*, 851-865. doi:10.2147/IJN.S296513

Setsukinai, K., Urano, Y., Kakinuma, K., Majima, H. J., & Nagano, T. (2003). Development of novel fluorescence probes that can reliably detect reactive oxygen species and distinguish specific species. *J Biol Chem, 278*(5), 3170-3175. doi:10.1074/jbc.M209264200

Silva, J. S., Georgiade, G. S., Dilley, W. G., McCarty, K. S., Sr., Wells, S. A., Jr., & McCarty, K. S., Jr. (1983). Menstrual cycle-dependent variations of breast cyst fluid proteins and sex steroid receptors in the normal human breast. *Cancer, 51*(7), 1297-1302. doi:10.1002/1097-0142(19830401)51:7<1297::aid-cncr2820510720>3.0.co;2-z

Song, Q. K., Li, J., Huang, R., Fan, J. H., Zheng, R. S., Zhang, B. N., . . . Chen, W. Q. (2014). Age of diagnosis of breast cancer in china: almost 10 years earlier than in the United States and the European union. *Asian Pac J Cancer Prev, 15*(22), 10021-10025. doi:10.7314/apjcp.2014.15.22.10021

Stangl, S., Gehrmann, M., Dressel, R., Alves, F., Dullin, C., Themelis, G., . . . Multhoff, G. (2011). In vivo imaging of CT26 mouse tumours by using cmHsp70.1 monoclonal antibody. *J Cell Mol Med, 15*(4), 874-887. doi:10.1111/j.1582-4934.2010.01067.x

Stangl, S., Gehrmann, M., Riegger, J., Kuhs, K., Riederer, I., Sievert, W., . . . Multhoff, G. (2011). Targeting membrane heat-shock protein 70 (Hsp70) on tumors by cmHsp70.1 antibody. *Proc Natl Acad Sci U S A, 108*(2), 733-738. doi:10.1073/pnas.1016065108

Stangl, S., Tei, L., De Rose, F., Reder, S., Martinelli, J., Sievert, W., . . . Multhoff, G. (2018). Preclinical Evaluation of the Hsp70 Peptide Tracer TPP-PEG24-DFO[(89)Zr] for Tumor-Specific PET/CT Imaging. *Cancer Res, 78*(21), 6268-6281. doi:10.1158/0008-5472.CAN-18-0707

Stangl, S., Tontcheva, N., Sievert, W., Shevtsov, M., Niu, M., Schmid, T. E., . . . Multhoff, G. (2018). Heat shock protein 70 and tumor-infiltrating NK cells as prognostic indicators for patients with squamous cell carcinoma of the head and neck after radiochemotherapy: A multicentre retrospective study of the German Cancer Consortium Radiation Oncology Group (DKTK-ROG). *Int J Cancer, 142*(9), 1911-1925. doi:10.1002/ijc.31213

Sung, H., Ferlay, J., Siegel, R. L., Laversanne, M., Soerjomataram, I., Jemal, A., & Bray, F. (2021). Global Cancer Statistics 2020: GLOBOCAN Estimates of

Incidence and Mortality Worldwide for 36 Cancers in 185 Countries. *CA Cancer J Clin, 71*(3), 209-249. doi:10.3322/caac.21660

Taraborrelli, S. (2015). Physiology, production and action of progesterone. *Acta Obstet Gynecol Scand, 94 Suppl 161*, 8-16. doi:10.1111/aogs.12771

Tsurutani, J., Iwata, H., Krop, I., Janne, P. A., Doi, T., Takahashi, S., . . . Li, B. T. (2020). Targeting HER2 with Trastuzumab Deruxtecan: A Dose-Expansion, Phase I Study in Multiple Advanced Solid Tumors. *Cancer Discov, 10*(5), 688-701. doi:10.1158/2159-8290.CD-19-1014

Vilchis-Juarez, A., Ferro-Flores, G., Santos-Cuevas, C., Morales-Avila, E., Ocampo-Garcia, B., Diaz-Nieto, L., . . . Gomez-Olivan, L. (2014). Molecular targeting radiotherapy with cyclo-RGDFK(C) peptides conjugated to 177Lu-labeled gold nanoparticles in tumor-bearing mice. *J Biomed Nanotechnol, 10*(3), 393-404. doi:10.1166/jbn.2014.1721

Vulczak, A., Catalao, C. H. R., Freitas, L. A. P., & Rocha, M. J. A. (2019). HSP-Target of Therapeutic Agents in Sepsis Treatment. *Int J Mol Sci, 20*(17). doi:10.3390/ijms20174255

Wang, C., Qian, J., Wang, K., Yang, X., Liu, Q., Hao, N., . . . Huang, X. (2016). Colorimetric aptasensing of ochratoxin A using Au@Fe3O4 nanoparticles as signal indicator and magnetic separator. *Biosens Bioelectron, 77*, 1183-1191. doi:10.1016/j.bios.2015.11.004

Wang, F., Wang, L., Qu, C., Chen, L., Geng, Y., Cheng, C., . . . Chen, Z. (2021). Kaempferol induces ROS-dependent apoptosis in pancreatic cancer cells via TGM2-mediated Akt/mTOR signaling. *BMC Cancer, 21*(1), 396. doi:10.1186/s12885-021-08158-z

Wang, H., & Zhang, X. (2019). ROS Reduction Does Not Decrease the Anticancer Efficacy of X-Ray in Two Breast Cancer Cell Lines. *Oxid Med Cell Longev, 2019*, 3782074. doi:10.1155/2019/3782074

Wanotayan, R., Chousangsuntorn, K., Petisiwaveth, P., Anuttra, T., Lertchanyaphan, W., Jaikuna, T., . . . Boonsang, S. (2022). A deep learning model (FociRad) for automated detection of gamma-H2AX foci and radiation dose estimation. *Sci Rep, 12*(1), 5527. doi:10.1038/s41598-022-09180-2

Weidle, U. H., Maisel, D., Klostermann, S., Schiller, C., & Weiss, E. H. (2011). Intracellular proteins displayed on the surface of tumor cells as targets for therapeutic intervention with antibody-related agents. *Cancer Genomics Proteomics, 8*(2), 49-63. Retrieved from https://www.ncbi.nlm.nih.gov/pubmed/21471515

Wen, K. K., Han, S. S., & Vyas, Y. M. (2020). Wiskott-Aldrich syndrome protein senses irradiation-induced DNA damage to coordinate the cell-protective Golgi dispersal response in human T and B lymphocytes. *J Allergy Clin Immunol, 145*(1), 324-334. doi:10.1016/j.jaci.2019.09.026

Weng, Y., Wang, H., Li, L., Feng, Y., Xu, S., & Wang, Z. (2021). Trem2 mediated Syk-dependent ROS amplification is essential for osteoclastogenesis in periodontitis microenvironment. *Redox Biol, 40*, 101849. doi:10.1016/j.redox.2020.101849

Xu, D., Yao, J., Zhang, Y., Xiao, N., Peng, P., Li, Z., . . . Yao, Z. (2020). The Effect of PEI-Mediated E1A on the Radiosensitivity of Hepatic Carcinoma Cells. *Asian Pac J Cancer Prev, 21*(4), 911-917. doi:10.31557/APJCP.2020.21.4.911

Xu, Y., Ji, Y., Li, X., Ding, J., Chen, L., Huang, Y., & Wei, W. (2021). URI1 suppresses irradiation-induced reactive oxygen species (ROS) by activating autophagy in hepatocellular carcinoma cells. *Int J Biol Sci, 17*(12), 3091-3103. doi:10.7150/ijbs.55689

Yalcin, Y., Tekin, I. O., & Tigli Aydin, R. S. (2022). Ionizing radiation induced DNA damage via ROS production in nano ozonized oil treated B-16 melanoma and OV-90 ovarian cells. *Biochem Biophys Res Commun, 615*, 143-149. doi:10.1016/j.bbrc.2022.05.030

Yao, Y., Chu, Y., Xu, B., Hu, Q., & Song, Q. (2019). Radiotherapy after surgery has significant survival benefits for patients with triple-negative breast cancer. *Cancer Med, 8*(2), 554-563. doi:10.1002/cam4.1954

Yin, L., Duan, J. J., Bian, X. W., & Yu, S. C. (2020). Triple-negative breast cancer molecular subtyping and treatment progress. *Breast Cancer Res, 22*(1), 61. doi:10.1186/s13058-020-01296-5

Yuan, L. Q., Wang, C., Lu, D. F., Zhao, X. D., Tan, L. H., & Chen, X. (2020). Induction of apoptosis and ferroptosis by a tumor suppressing magnetic field through ROS-mediated DNA damage. *Aging (Albany NY), 12*(4), 3662-3681. doi:10.18632/aging.102836

Zhang, C., Li, S., & Zhao, Z. (2022). beta-Elemene Promotes Apoptosis Induced by Hyperthermia via Inhibiting HSP70. *Dis Markers, 2022*, 7313026. doi:10.1155/2022/7313026

Zhang, L., Tang, R., Deng, J. P., Zhang, W. W., Lin, H. X., Wu, S. G., & He, Z. Y. (2020). The effect of postmastectomy radiotherapy in node-positive triple-negative breast cancer. *BMC Cancer, 20*(1), 1146. doi:10.1186/s12885-020-07639-x

Zhang, Z., Lu, M., Chen, C., Tong, X., Li, Y., Yang, K., . . . Qin, L. (2021). Holo-lactoferrin: the link between ferroptosis and radiotherapy in triple-negative breast cancer. *Theranostics, 11*(7), 3167-3182. doi:10.7150/thno.52028

Zhang, Z., Zhang, H., Li, D., Zhou, X., Qin, Q., & Zhang, Q. (2021). Caspase-3-mediated GSDME induced Pyroptosis in breast cancer cells through the ROS/JNK signalling pathway. *J Cell Mol Med, 25*(17), 8159-8168. doi:10.1111/jcmm.16574

Zhao, R. Z., Jiang, S., Zhang, L., & Yu, Z. B. (2019). Mitochondrial electron transport chain, ROS generation and uncoupling (Review). *Int J Mol Med, 44*(1), 3-15. doi:10.3892/ijmm.2019.4188

10. Acknowledgement

Over the past three years, the COVID-19 pandemic has made it a challenging period for me as a doctoral researcher. Despite the difficulties, it was also an exciting time for me. I sincerely appreciate the support and collaboration from others without which it would have been difficult for me to complete my doctoral thesis. Here I would sincerely thank to them in the following paragraphs.

My heartfelt thanks go to Professor Gabriele Multhoff for offering me the chance to pursue my doctoral studies in her group. She offers me supports from all sides. Throughout the process of conducting experiments and writing the paper, we had numerous discussions. The thriving discussions always inspired me to gain more insights into my project.

I am also grateful to Professor Agnes Goerlach. She is my mentor at the Technical University of Munich. She took part in my Thesis Committee meetings and gave me valuable feedback.

Here I also want to thank Stefan Stangl, Alicia Hernandez-Schnelzer, Fei Wang, Mina Yazdi, Morteza Hasanzadeh Kafshgari and Ali Bashiri Dezfouli, they helped me a lot with my project. They showed me how to use the instruments in our lab when I was new here. They offered unselfish support and help when I need help in my project.

My deepest gratitude goes to my family. I haven't been home for 4 years because of COVID-19. My wife Ru Zhang is always by my side, we share joys and sorrows together. We took care of each other when we got COVID-19 in 2022. Although I

haven't seen my parents, brother and nephews for years, they have consistently supported both my research and my life in Germany.